Ceramics International 48 (2022) 2212–2229

Contents lists available at ScienceDirect

Ceramics International

journal homepage: www.elsevier.com/locate/ceramint

Metakaolin-based geopolymers: Efflorescence and its effect on microstructure and mechanical properties

Márlon A. Longhi [a,*], Erich D. Rodríguez [b], Brant Walkley [c,d], Diego Eckhard [e], Zuhua Zhang [f,g,**], John L. Provis [c], Ana P. Kirchheim [a]

[a] Department of Civil Engineering, Post-Graduate Program in Civil Engineering: Construction and Infrastructure, Universidade Federal do Rio Grande do Sul (NORIE/UFRGS), Av. Osvaldo Aranha, 99. 3º andar, Porto Alegre, Brazil
[b] Department of Structures and Civil Construction. Technology Centre, Universidade Federal de Santa Maria (UFSM), Santa Maria, Av. Roraima 1000, Prédio 10A, RS, Brazil
[c] Department of Materials Science and Engineering, Sir Robert Hadfield Building, The University of Sheffield, Sheffield, S1 3JD, UK
[d] Department of Chemical and Biological Engineering, Sir Robert Hadfield Building, The University of Sheffield, Sheffield, S1 3JD, UK
[e] Department of Pure and Applied Mathematics. Universidade Federal do Rio Grande do Sul (UFRGS), Av. Bento Gonçalves, 9500, Prédio 43-111, Porto Alegre, Brazil
[f] Key Laboratory for Green & Advanced Civil Engineering Materials and Application Technology of Hunan Province, College of Civil Engineering, Hunan University, Changsha 410082, PR China
[g] Key Laboratory of Building Safety and Energy Efficiency of Ministry of Education, Hunan University, Changsha, 410082, PR China

ARTICLE INFO

Keywords:
Geopolymer
Metakaolin
Efflorescence
Leaching
Mechanical properties
Durability

ABSTRACT

Efflorescence in geopolymers results from mobility of excess alkali and consequent crystallization of alkali carbonates. Efflorescence potential of various geopolymers has been reported previously but the knowledge regarding the effect of efflorescence on the microstructure and mechanical properties of geopolymers remains limited. In this work, metakaolin-based geopolymers were exposed to air, partially immersed in water, and fully immersed, to simulate different processes involved in efflorescence formation. The mechanical properties were assessed by compressive, splitting tensile and flexural strengths, and linear deformation. The microstructural features were investigated by SEM, synchrotron XRD, multinuclear MAS NMR, MIP and synchrotron X-ray microtomography. Extensive efflorescence resulted in a reduction of mechanical strength and changes in the nanostructure and microstructure, which is different from observations for Portland cement-based materials, where efflorescence is usually regarded as a surface or aesthetic problem. The understanding of the relationship between efflorescence formation, the synthesis and exposure conditions provides important insight into the manufacturing and application conditions of geopolymer related materials.

1. Introduction

Efflorescence formation is a visible phenomenon observed mostly on the surface of cementitious and ceramic materials, usually causing mainly aesthetic damage or superficial deterioration. In geopolymers, efflorescence formation is still not fully understood due to the different mechanisms of reaction and product formation. Geopolymer formation involves the reaction (often called “activation”) of reactive aluminosilicate materials with highly alkaline solutions (or ‘activators’) [1,2]. Thus, geopolymers contain high amounts of alkali metals. Alkalis are primarily present in the disordered reaction product, an alkali aluminosilicate hydrate gel denoted M-A-S-(H) gel, with M representing alkali metals, most commonly Na^+ or K^+ [3]. Alkali cations in the M-A-S-(H) gel neutralize the excess negative charge resulting from Al in tetrahedral coordination in the alkali aluminosilicate gel framework [3], forming Na–O–Al(Si) linkages. Thus, at stoichiometric equilibrium the M-A-S-(H) gel will exhibit an Na/Al ratio of 1.0 [4]. However, sodium can also be bound weakly to the gel as $Na(H_2O)_n^+$ in the pore solution [5,6]. Some of these forms are weakly bounded under certain conditions, resulting in free/leachable alkalis as measured by leaching, as reported in previous studies [7,8]; leachable alkali values between 1 and 25% of the total alkali content in the geopolymers were reported. In a

* Corresponding author.
** Corresponding author. Key Laboratory for Green & Advanced Civil Engineering Materials and Application Technology of Hunan Province, College of Civil Engineering, Hunan University, Changsha, 410082, PR China.
E-mail address: marlonlonghi@gmail.com (M.A. Longhi).

https://doi.org/10.1016/j.ceramint.2021.09.313
Received 29 June 2021; Received in revised form 13 September 2021; Accepted 30 September 2021
Available online 2 October 2021

Table 1
Formulation of geopolymer samples.

Geopolymer	Silica modulus (MS)	Curing temperature (°C)	Materials (g)			
			MK	NaOH	SS[a]	H_2O
MS_1.5	1.5	25	100	7.1	98.7	24.9
MS_1.0	1.0	25	100	13.3	65.8	44.8
MS_0.5	0.5	25	100	19.6	32.9	63.7
MS_0.0	0.0	25	100	25.8	0.0	75.5
MS_1.0_50°	1.0	50	100	13.3	65.8	44.8

[a] SS: Sodium silicate solution.

previous analysis of leaching potential of metakaolin-based geopolymers using an ionic equilibrium method, around 55% of alkalis were observed to be weakly bounded and 45% were stable in the framework structure [9]. These high values of potentially leachable alkalis have raised concerns regarding extensive efflorescence and consequent damage in geopolymer cements.

Efflorescence formation occurs from free alkali mobility in geopolymers. Capillary pressure induces water transport and alkali movement via both diffusive and convective processes, the latter of which is accelerated when the material is exposed to wetting/drying cycles. The pore size distribution also plays an important role in this movement, as larger pores are more likely to be connected by microcracks and contribute to the faster alkali leaching [8]. Alkali leaching can also be damaging to the M-A-S-(H) gel structure due to the nanostructural transformation associated with removal of alkalis and consequent changes of the chemical environment of Al^{IV} species [9]. After leaching, the alkali metals present in solution react with HCO_3^- or CO_3^{2-} (resulting from dissolved atmospheric CO_2) to form alkali carbonate phases. This process is commonly referred to as carbonation, and is mainly controlled by the dissolution and diffusivity of CO_2. Both of these factors are a function of the concentration (or partial pressure) of CO_2 in the atmosphere at the air/pore fluid interface, and the diffusivity is also related to the interconnectivity of pore structure (which is a function of porosity [10]) and exposure conditions [11]. A partially saturated moisture condition accelerates the carbonation reaction process, where relative humidity (RH) values of 65 ± 5% were observed as the pessimum in GBFS/MK-based geopolymers [12]. Depending on the porosity, alkali concentration of geopolymers, and diffusivity of CO_2, the deposition of alkali carbonates can be internal (subflorescence) or external (efflorescence) [13]. Subflorescence can generate an internal pressure resulting from crystallization of the alkali carbonate phases, and this can affect the structural integrity of matrix [13].

The products formed in efflorescence are predominantly carbonates associated with the alkali used in the activator. The formation of a hydrated sodium carbonate ($Na_2CO_3{\cdot}7H_2O$) [8,14], sodium bicarbonate ($NaHCO_3$) [7] and natrite (Na_2CO_3) [15] have all been previously observed. Visible formation of alkali carbonate crystals is also related to RH in the air. Low values of RH reduce dissolution and diffusion of atmospheric CO_2, whereas high values of RH can dissolve the carbonate crystals formed. This crystallization occurs at a specific RH equilibrium, which is dependent on the type of carbonate crystal formed [16,17]. Thus, efflorescence formation is a phenomenon associated with different processes and their effects are dependent on the geopolymer properties and microstructure, exposure conditions, and magnitude/type of carbonate crystallization.

In previous studies, the effect of efflorescence formation was evaluated for some specific geopolymeric materials and conditions, with efflorescence formation observed to reduce the compressive strength of the binder [13,18]. In fly ash-slag based alkali-activated materials, alkali leaching processes have been observed to not lead to a reduction of compressive strength, but do hinder ongoing strength and microstructural development over time [18]. In the same study, shrinkage was more evident in samples with efflorescence formation, than in those subjected to alkali leaching without efflorescence formation. Other work, using metakaolin as precursor, attributed microstructural changes to excessive alkali leaching [9]. Using three different fly ashes, Zhang et al. [13] evaluated the compressive strengths of geopolymers in contact with air, partially immersed in water, and fully immersed. Their results showed an increase of compressive strength for samples in air and a reduction for samples partially or fully immersed in water. The negative influence of efflorescence formation was attributed to multiple factors including loss of alkalis from the M-A-S-(H) gel and subflorescence formation. However, compressive strength evaluation is not the best option to assess the impact of efflorescence because the crystallization of carbonates causes a internal expansion. Instead, tensile and flexural strength should be more suitable from the perspective of mechanical impact.

This study aims to evaluate the effect of efflorescence formation, air carbonation and alkali leaching on the mechanical and microstructural properties of metakaolin-based geopolymers. This is assessed under conditions relevant to the most common industrial settings for geopolymer cement use. The findings discussed are crucial to fully understand efflorescence in geopolymer cements.

2. Experimental

2.1. Materials and sample preparation

The metakaolin (MK) used as precursor to make geopolymers had a mean particle size of 4.56 μm, specific surface area of 13.49 m^2/g and consisted of 54.82% wt.% SiO_2, 42.57 wt% Al_2O_3 and 0.11 wt% loss on ignition at 1000 °C. The complete characterization and more detailed description were previously reported [9].

Alkali activators used were analytical grade NaOH (~99%) dissolved in water, and a sodium silicate solution with 29.4 wt% SiO_2, 14.7 wt% Na_2O and 52.7 wt% H_2O, supplied by PQ Australia. The composition of the alkali activator was adjusted by blending the NaOH and sodium silicate solution to reach the desired molar ratios.

The formulations of the geopolymers were based on previous reports [9,19]; materials were formulated with an alkali concentration of 20 wt % of Na_2O with respect to the mass of precursor, and used activators with silica modulus values (MS, SiO_2/Na_2O ratio in the activator) of 1.5, 1.0, 0.5, and 0.0. The content of water was adjusted to give a water/-binder ratio of 0.55, where binder represents the MK and the anhydrous fraction of the alkali activator. Mixes were designed to provide a range of geopolymer physical and chemical properties. The pastes were produced by mechanical mixing for 5 min, then stored in a sealed plastic container at room temperature (~25 °C) and RH ≥ 90% for 28 days, before starting the exposure. To assess the effect of thermal curing, the geopolymer produced with MS = 1.0 was also cured at 50 °C for 24 h, and then stored at room temperature for 27 days. Table 1 shows the ID assigned to each formulation.

After 28 days of curing, samples were exposed to different exposure conditions for an additional 28 days. Fig. 1 shows a representation of exposure conditions to cylindrical, for the execution of other mechanical test, cubic and prismatic samples were also used. As a **reference** system (without any contact with air, moisture or damaging environment), the samples were kept completely sealed in a closed container until the date of testing at 25 ± 5 °C. Samples were exposed to **efflorescence** by the partial immersion of the sample (to ~5 mm depth) in distilled water, with the remainder of the sample open in ambient conditions (25 ± 5 °C and RH = 65 ± 15%). In this exposure condition, for cubic and prismatic samples used for the other tests, the longer side of the specimen was placed in contact with water, and for testing, lateral surfaces were used. Additionally, efflorescence crystals were removed carefully from the surface to prevent any interference. The level of water was adjusted every 24 h. As a third condition, the development of **natural carbonation** where the sample is in contact with the air under natural conditions (higher CO_2 concentration, when compared to the reference system), the carbonation process is developed near the sample surface.

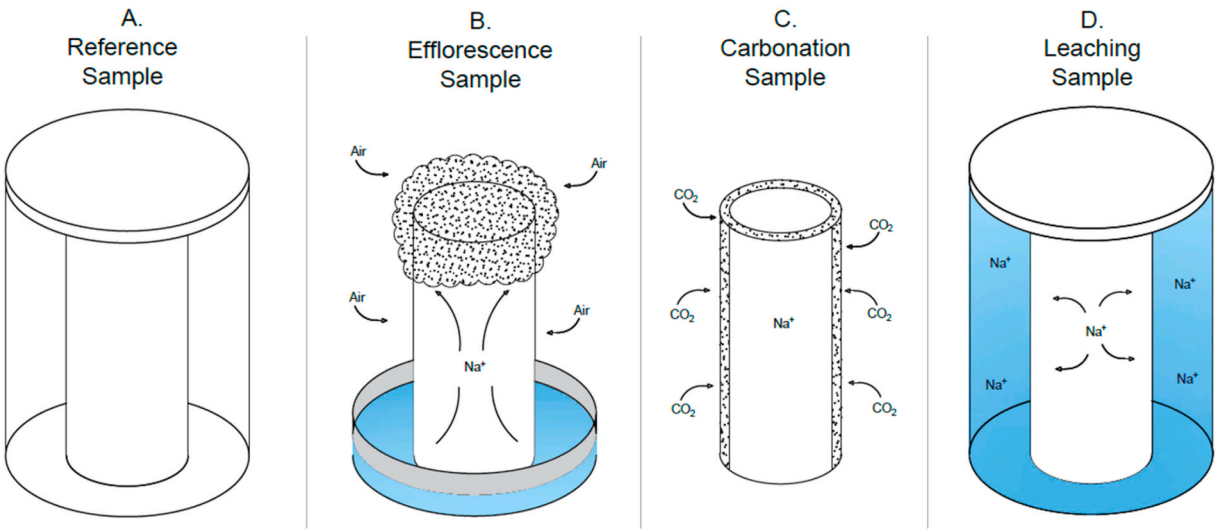

Fig. 1. Different conditions of ambient exposure (A. reference system, B. efflorescence, C. carbonation system, and D. leaching).

The **leaching** conditions, as the fourth exposure condition tested, were developed by the complete immersion of the sample in deionized water in a proportion in mass of 1/20 (geopolymer/water) in a sealed vessel.

2.2. Tests conducted

After 28 days of curing, followed by 28 days of exposure (Fig. 1), the samples were dried and placed in ambient conditions (~25 °C and RH = 65 ± 15%) for 24 h. The analyses conducted were:

- **Compressive strength** of five replicate cubic samples of 20 mm of height for each system and exposure condition. The test was conducted using an MTS universal mechanical testing machine with a cross-head speed of 0.5 mm/min. For the mechanical tests, the samples exposed to the efflorescence formation (Fig. 1B) were tested according to the capillary water suction, where the load applied was in the bottom/immersed and top/air-exposed surfaces.
- **Splitting tensile strength** of four replicate cylindrical samples with 20 mm diameter and 35 mm height. For this analysis the samples were tested in the longitudinal direction. The splitting tensile strength was calculated using the equation according to NBR 7222, 2011, Eq. (1):

$$\text{Splitting tensile strength (MPa)} = f_t = \frac{2P}{\pi DL} \quad (1)$$

where P is the load applied to the sample in N, D is the diameter in mm and L is the height in mm. A tape of neoprene of 2 mm thickness was used to homogeneously distribute the load.

- **Flexural strength** of three replicate prismatic samples of 20 × 20 × 80 mm, tested in 3-point bending geometry. The flexural strength was calculated using Eq. (2) according to NBR 12142, 2010:

$$\text{Flexural strength (MPa)} = f_f = \frac{3PL}{2bd^2} \quad (2)$$

where P is the load applied in N, L is the length of the support span, b is width, d is thickness. The prismatic sample exposed to the efflorescence formation (Fig. 1B) were loaded in the lateral surfaces, with a span length of 80 mm.

- **Linear deformation** was measured for prismatic samples of 20 × 20 × 80 mm using a length comparator along the longitudinal direction for each exposure condition. The initial measurement was made after 28 days of cure, and then after another 28 and 56 days of exposure in each exposure condition. The samples were exposed in the same way of flexural strength samples.

Microstructural features were evaluated using:

- **High resolution scanning electron microscopy (SEM)** using a FEI Quanta 650 FEG, in the Brazilian Nanotechnology National Laboratory LNNano (Laboratório Nacional de Nanotecnologia). The equipment was equipped with an Everhart Thomley SED (secondary electron detector) and an in-column detector (ICD) for secondary electrons in BD mode, working with a high resolution Schottky field emission source (FEG), accelerating voltage between 200 V and 30 kV, and a probe current ≤ 200 nA. The samples used were superficial fragments of the specimens, where the external part of the fragment was analyzed. Each sample was dried at 60 °C for 2 h, placed on a carbon tab, and coated with gold for 60 s with a current of 40 A.
- **Solid-state single pulse ^{23}Na, ^{27}Al and ^{29}Si magic angle spinning (MAS) NMR spectroscopy** using a Bruker Avance III HD 500 spectrometer at 11.7 T (B_0) with a 4.0 mm dual resonance CP/MAS probe, yielding a Larmor frequency of 132.26 MHz for ^{23}Na, 130.32 MHz for ^{27}Al and 99.35 MHz for ^{29}Si. ^{23}Na MAS NMR spectra were collected with a 3.0 μs non-selective (π/2) excitation pulse, a measured 10 s relaxation delay, a total of 128 scans, and spinning at 12.5 kHz ^{27}Al MAS NMR spectra were collected with a 1.7 μs non-selective (π/2) excitation pulse, a measured 5 s relaxation delay, a total of 512 scans, and spinning at 12.5 kHz ^{29}Si MAS NMR spectra were acquired using a 5.5 μs non-selective (π/2) excitation pulse, a measured 60 s relaxation delay, a total of 256 scans, and spinning at 12.5 kHz. For all experiments, the spectrometer field was aligned to the ^{13}C resonance of adamantane at 38.48 ppm, and ^{23}Na, ^{27}Al and ^{29}Si spectra were referenced to 1.0 $NaCl_{(aq)}$, 1.0 mol/L $Al(NO_3)_{3(aq)}$ and neat tetramethylsilane (TMS), respectively, at 0 ppm. Gaussian peak profiles were used to deconvolute the ^{29}Si spectra, using the minimum number of peaks possible [20]. Peak intensities were required to be consistent with the structural constraints described by the thermodynamics of a statistical distribution of Si and Al sites within a Q^4 aluminosilicate network for (N,K)-A-S-H gel products [21].
- **X-ray diffraction (XRD)** using the XRD1 beamline at the Brazilian Synchrotron Light Laboratory (LNLS). The LNLS is a second-generation synchrotron source, which operates with an energy of 1.37 GeV. The XRD1 beamline is installed on the D12B bending magnet (1.67 T), mounted in a transmission geometry (Debye-Scherrer) with 24 Mythen 1 k linear detectors with 1280 pixels at 50 μm each, with a sampling rate of 2 kHz. The detectors are mounted at

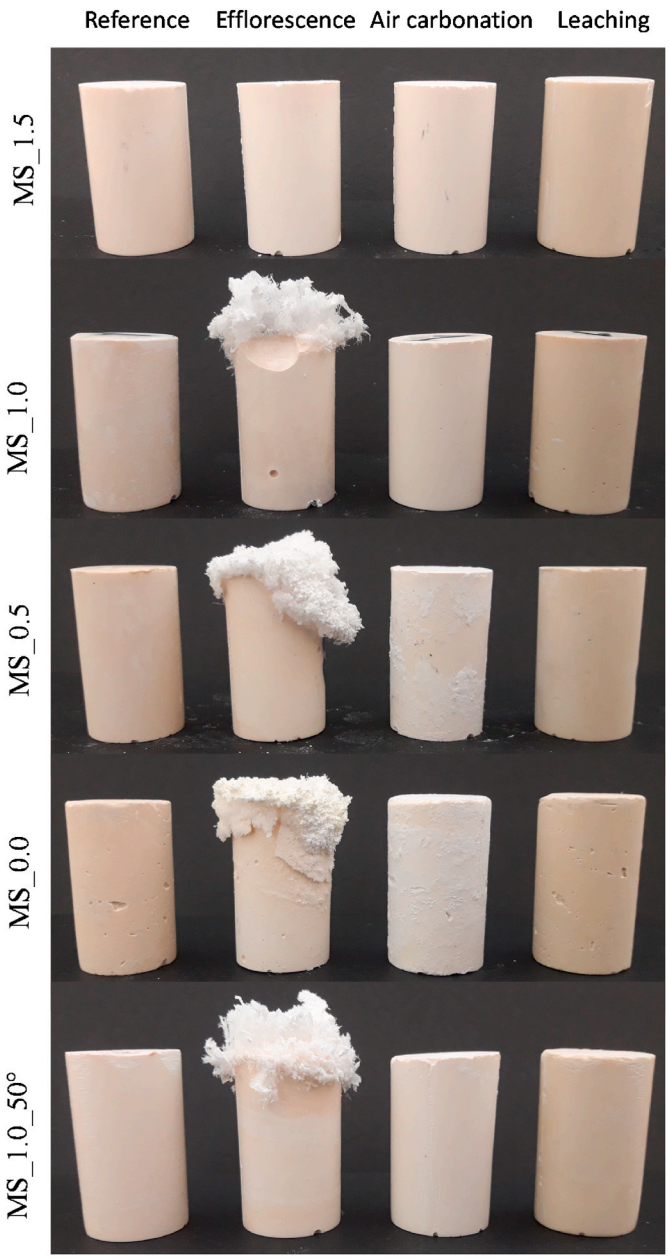

Fig. 2. Visual evidence of efflorescence formation in geopolymeric samples. (Cylindrical samples, with diameter 20 mm and height 35 mm).

a distance of 760 mm, generating an angular resolution of 0.0037°. The beamline energy was adjusted to 12 keV, equivalent to a wavelength of 1.033 Å, with a photon flux of about 10^9 photons/s, at 100 mA [22,23]. The data were then converted to equivalent Cu Kα 2θ angles for plotting, to enable comparison with the broader literature in which this conventional X-ray energy is used.

- **Thermogravimetric analysis (TGA) and simultaneous thermal analysis (STA)** using a Tam Air Discovery SDT 650, with a heating rate of 10 °C/min up to 1000 °C and 90 μL alumina crucibles and nitrogen as gas environment.
- **X-ray microtomography (XRμT)** using the Brazilian synchrotron LNLS (Laboratório Nacional de Luz Síncrotron) at Campinas, using beamline IMX [24]. A monochromatic beam of 4 to 20 k eV with a pixel size of 0.82 μm^2 and field view (horizontal × vertical) of 1.64 mm^2. As detector a 7.4 μm pixel, 2048 × 2048 pixel, 14-bit CCD (PCO.2000) camera was used. Tomographic images were obtained point-to-point with an angle range of 360° along its vertical axis with a step size of 0.1758° (or 2048 projections), to achieve up to 310000 counts. Three Si(111) filters were used, consisting one of 200 μm and two of 350 μm in order to reduce the beam-hardening effects [25]. Based on the configuration of the beamline and parameters conditions, the images acquiring in the XRμT are limited to 0.84 μm per voxel/pixel. Cylindrical geopolymer samples of ~1.70 mm diameter were produced, cured and treated (RE, EF and LE) under the same conditions as described previously. Sample heights were between ~7 and 11 mm and the beam was adjusted approximately in the middle of the specimen. A set of images 3072 × 3072 × 2048 were obtained and adjusted for 3D volume generation [26]. In order to reduce the size of the data to be analyzed, a prismatic region of interest of 1024 × 512 × 512 voxels was extracted. The images and segmentation analyses were executed using Avizov 9.5.0 software package and adjusted using different filter plug-in tools based on the variation on grey scale intensity.

3. Efflorescence formation

3.1. Visual efflorescence

Fig. 2 shows the visual aspect of geopolymers under different exposure conditions after 28 days of curing and then 28 days of exposure. The samples under reference conditions (RE) did not show any efflorescence formation for any of the geopolymers assessed.

When the samples were in contact with water at one end (EF), most of the systems exhibited efflorescence formation on the surface, which corresponds to carbonate-type products as was identified previously [19]. The images in Fig. 2 show that the content of sodium silicate in the alkali activator plays an important role in the reduction of efflorescence formation. Geopolymer MS_1.5 does not show any efflorescence formation, while MS_0.0 (hydroxide-activated geopolymer) shows severe carbonate formation and surface deterioration. This behavior was classified by Zhang et al. [13] as subflorescence, which can be attributed to the crystallization of carbonate within the pore structure of the near-surface layer inducing stress and subsequent cracking. Additionally, in the geopolymers MS_1.0 and MS_0.0, Fig. 2 shows the presence of some broken parts, which can be attributed to the internal crystallization and excessive internal stress within the pore network. As observed in previous studies [9,19], the use of silicate-rich activators reduces the amount of leachable alkalis, which is due to the higher density and lower porosity when compared to geopolymers with lower contents of soluble silicate [3]. The use of higher curing temperature (50 °C for 24 h) did not yield an observable reduction in efflorescence formation; the heat-cured samples showed similar behavior to the corresponding geopolymers cured at room temperature (MS_1.0).

The samples exposed to the air carbonation conditions (CA), where a natural carbonation process is induced, also showed a thin layer of carbonate deposition distributed in the sample (not only on the top of the specimens). The high porosity of these systems allows the movement of water and free alkalis to the surface, which contributes to the development of efflorescence. Taking into account the lack of an external supply of water, the formation of carbonate-type products on the surface is less severe when compared to partially immersed samples.

The samples exposed to leaching conditions (LE) do not show any visible surface change, however, the contact with water induces the removal of free alkalis. Previous work observed the removal of around 17–30% of alkalis using cylindrical samples [19] and higher than 50% using powdered samples (hardened geopolymer that was ground previously) [9]. On the same way, the addition of sodium silicates and reduction of the content of activator can reduce the amount of sodium leached [27]. Due to the removal of alkalis by the leaching process, as well as the low concentration of dissolved CO_2 in the aqueous solution, the formation of efflorescence is not expected. However, the movement and quantity of leached alkalis is important for understanding the susceptibility of the material to efflorescence formation, and the effects

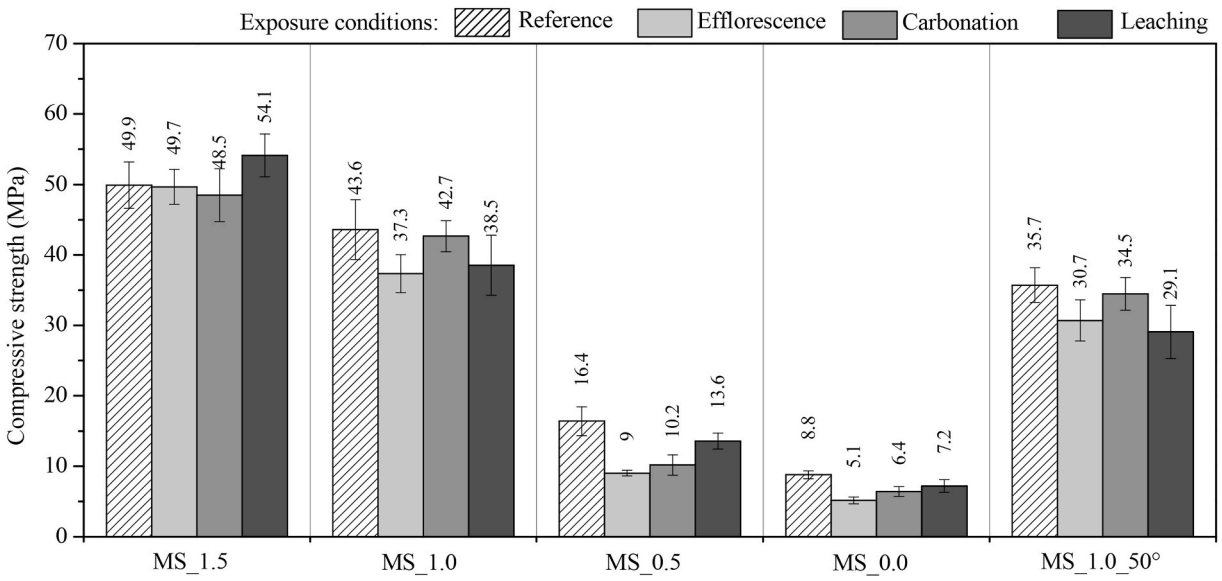

Fig. 3. Compressive strength of geopolymers in different conditions of exposure.

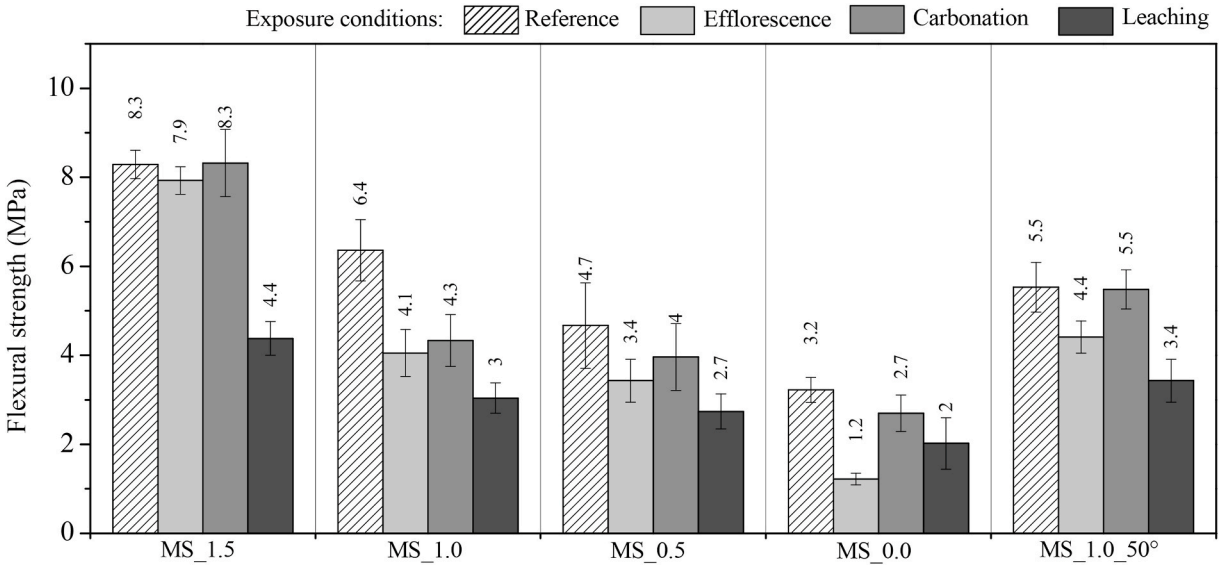

Fig. 4. Flexural strength of geopolymers in different conditions of exposure.

associated with alkali removal.

3.2. Compressive strength

The compressive strength of geopolymers after exposure to the specified conditions is shown in Fig. 3. Geopolymers produced with different contents of sodium silicate in the activator and under different curing conditions provide different levels of strength under reference (RE) conditions. The maximum value of compressive strength achieved was 49.9 MPa the geopolymer MS_1.5, which is up to 5.6 times higher compared to the geopolymer MS_0.0. This increase was discussed in previous studies [3,28,29] and was attributed to the high amount of Si in the M-A-S-(H) gel, resulting in denser and stronger microstructure. Fig. 3 also shows that in most cases the reference exposure conditions yield the highest compressive strength, indicating that the air carbonation, efflorescence-inducing conditions, and alkali leaching each have a detrimental effect on the mechanical performance of the geopolymers. The largest reduction is associated with efflorescence formation, where the highest reduction in most of the cases is observed mainly in the systems with the lower content of soluble silicates: MS_0.5 and MS_0.0, which lose up to 45% of their compressive strength compared to the reference samples.

The effect of exposure conditions was also evaluated in previous papers using fly ash-based systems [18,30], where a reduction in compressive strength was also reported under efflorescence conditions. According to Yao et al. [18], efflorescence formation induces carbonate crystallization and an internal stress can be developed. This behavior is also consistent with the subflorescence formation observed by Zhang et al. [13] and the phenomena observed in this study. The different levels of alkali leaching, environmental conditions and carbonate formation determine the level of degradation and the effect observed.

Even though the natural carbonation conditions (CA) seem to be less aggressive, as was shown in Fig. 2 for the geopolymers MS_0.5 and MS_0.0, a reduction of up to 38% in the compressive strength is observed. These geopolymer samples showed efflorescence formation as a homogeneous thin layer (~1 mm) covering the external surface. There

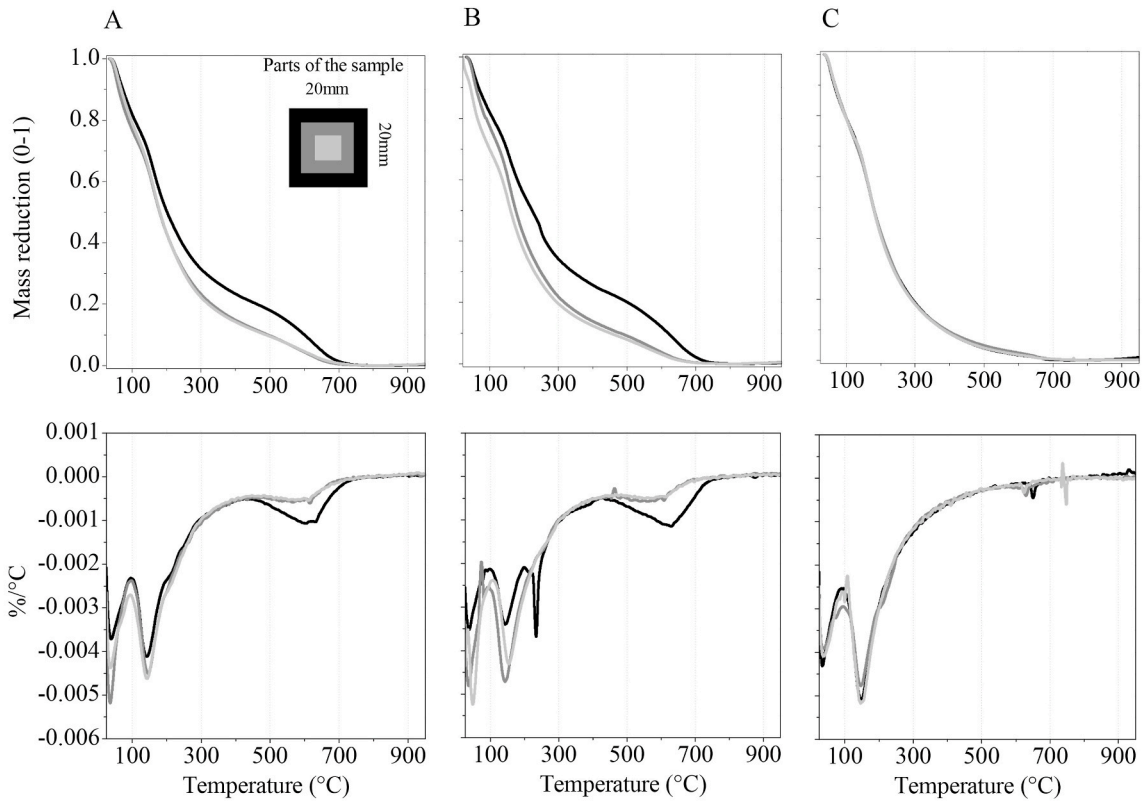

Fig. 5. TGA analysis of the geopolymer MS_0.5 exposed to different exposure conditions, sampled at different depths. A. Air carbonation, B. Efflorescence and C. Leaching.

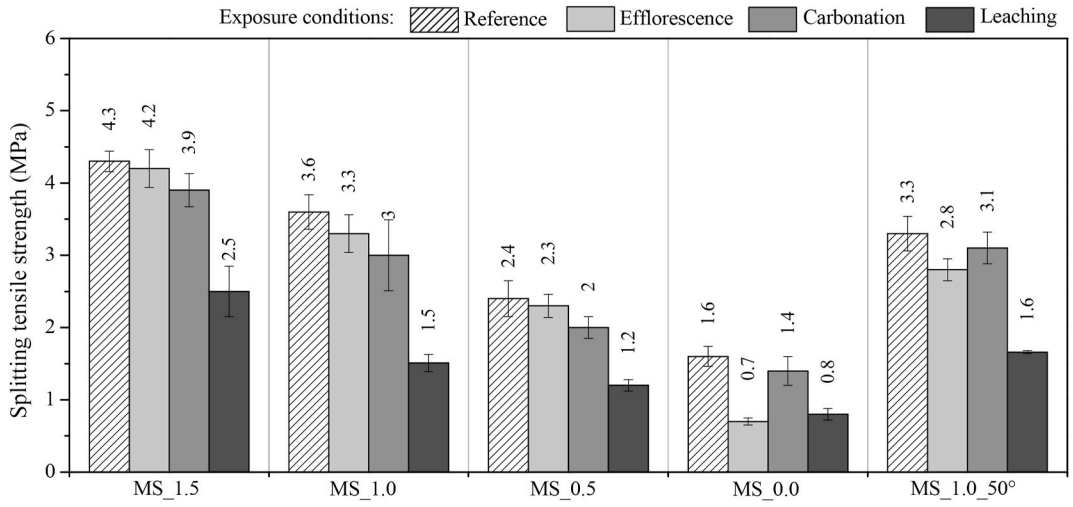

Fig. 6. Splitting tensile strength of geopolymers in different conditions of exposure.

is also potentially some deterioration of this external surface due to the formation of crystals into the pore network, which was also previously reported by Zhang et al. [13] as subflorescence formation. It is potentially relevant to note that a statistically significant loss of strength under carbonation conditions was observed only in the samples which had the lowest strengths under reference conditions. These will therefore be the samples that are the least able to resist internal mechanical forces generated either by crystallization or by drying action, and therefore are the most prone to damage and further loss of strength by these mechanisms.

For the leaching conditions (LE), a slight reduction of compressive strength was also observed for the geopolymers MS_0.5 and MS_1.0_50°. It is important to highlight that the geopolymer with the highest content of soluble silicate (MS_1.5) do not show notable loss of compressive strength, regardless of the exposure conditions.

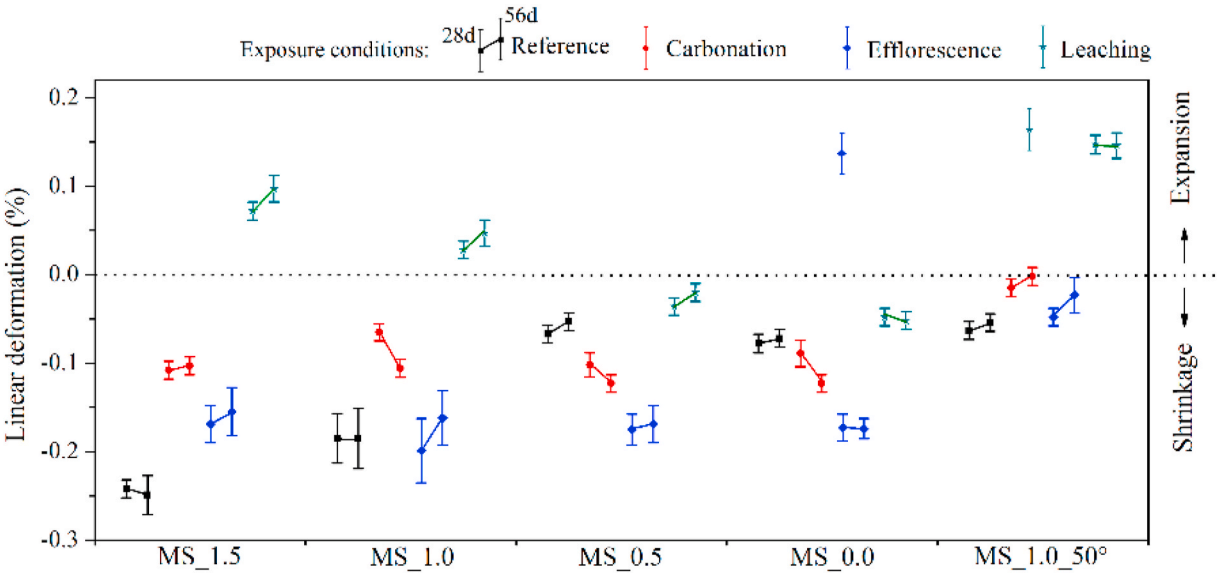

Fig. 7. Linear deformation of geopolymers in different conditions of exposure.

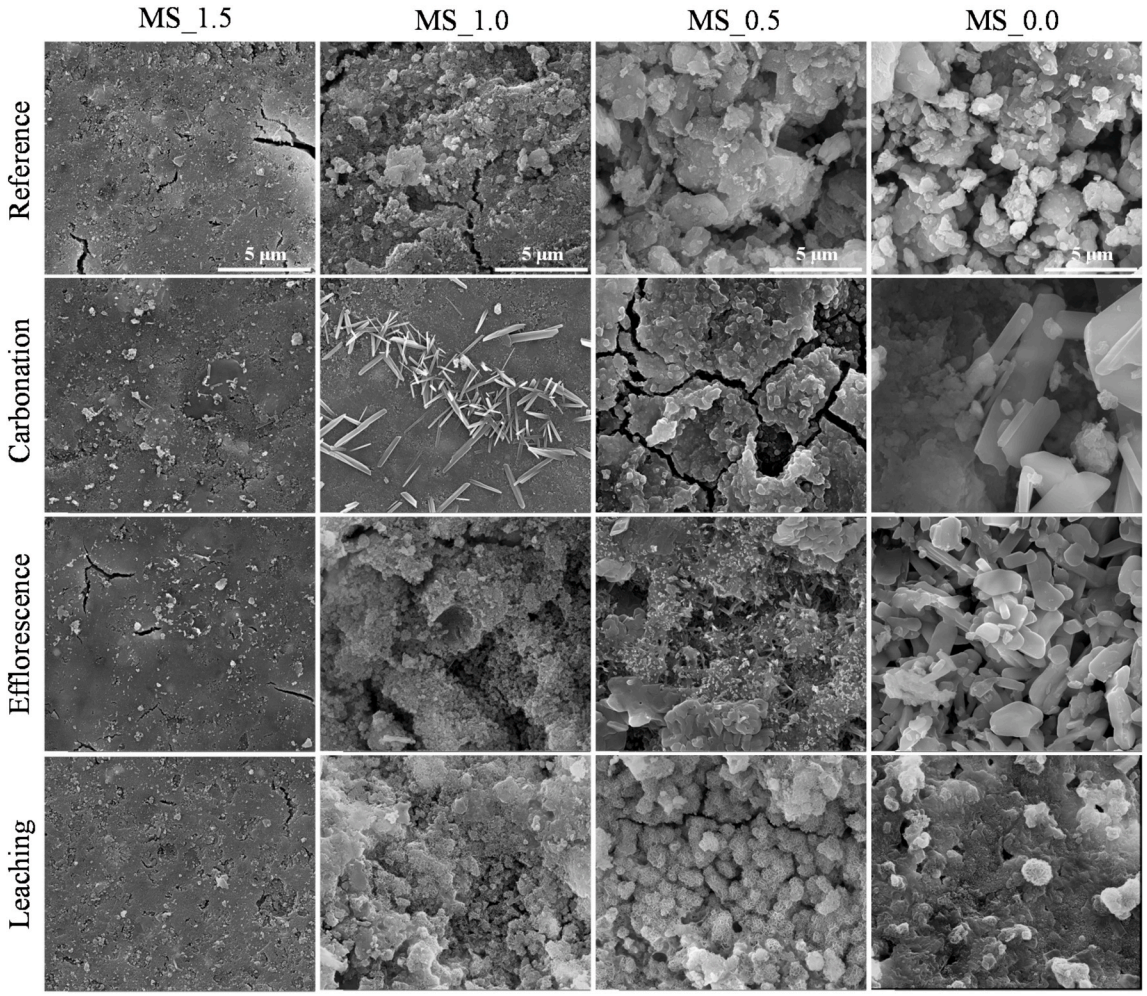

Fig. 8. SEM images of geopolymer samples (MS_1.5, MS_1.0, MS_0.5 and MS_0.0 as marked) in different exposure conditions. All micrographs are shown with the same magnification, as indicated by the scalebars in the top row of images.

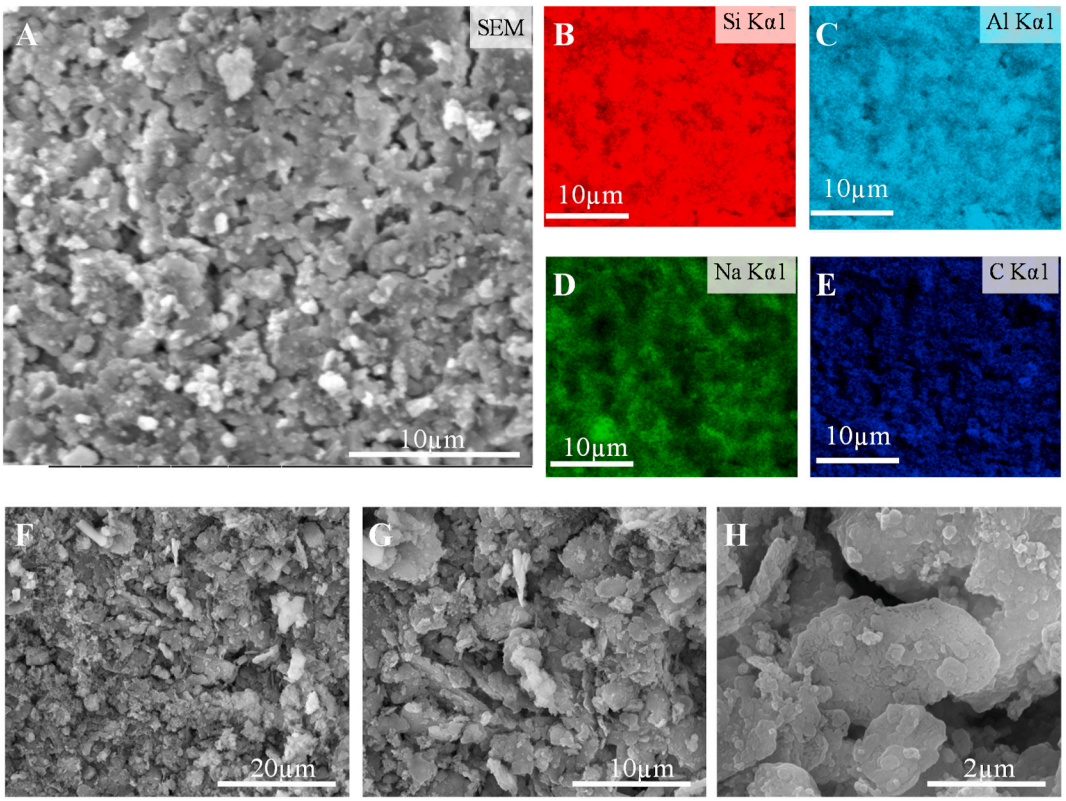

Fig. 9. SEM images (A, F, G, and H) and EDS elemental maps for Si (B); Al (C); Na(D) and C (E) of the geopolymer MS_0.5 exposed to reference condition and correspond to the closest part in the exposed surface.

3.3. Flexural strength

The flexural strength results, measured in 3-point bending geometry, are shown in Fig. 4. All the exposure conditions affect the flexural strength, although with potentially important differences from the trends observed in compressive strength data where the efflorescence formation and superficial carbonation can damage the material surface due to the excessive crystal formation in the surface and within the pores.

Interestingly, the most marked loss of flexural strength was observed under the leaching conditions. This behavior can be attributed to the alkali removal from the framework structure. This is associated to the leaching of free-alkali and some soluble compounds within the geopolymeric gel, as observed previously [9]. IN the same study was observed that the leaching process induces the reduction of Q^4(4Al) and Q^4(3Al) silicate sites within the geopolymeric matrix, indicating a structural change due to the alkali removal with some instability of sodium aluminosilicate gel under leaching; this will be addressed in detail in section 4.2 below.

Due to the open porosity and presence of a high amount of free alkalis in metakaolin-based geopolymers, the leaching exposure may be more uniform throughout the sample thickness than efflorescence and air carbonation conditions, particularly for the slender prismatic samples used for flexural strength testing. Therefore, the depth of geopolymer affected determines the reduction in tensile strength.

In order to understand this behavior, and the extent of the effect, the geopolymer system MS_0.5 after being submitted to the three exposure conditions was analyzed by TGA at three different depths, as shown in Fig. 5A (where the cross section of the sample is shown in the figure). Each TG/DTG curve corresponds to a sample collected in three different points from one specimen; the piece extracted (~5 g) was milled in an agate mortar, the reaction stopped using isopropanol, and dried in the oven for 45 min at 60 °C. To allow direct comparison between the depths in each exposure condition, the data were normalized between 0 and 1. The TG/DTG curves indicate the decomposition of carbonate phases at temperatures between 500 °C and 700 °C, which is clearer for the external fraction of samples (represented by the black line) exposed to air carbonation (CA) and efflorescence (EF) exposure conditions. A lower content of carbonate products, and therefore less carbonation, is observed in the samples extracted from the internal fraction (represented by grey lines). Therefore, the near-surface is more highly affected than the internal part when subjected to air contact and efflorescence formation. On the other hand, the extraction of free alkalis during the leaching process did not lead to carbonate formation (Fig. 5C). The TG profile is consistent throughout this sample independent of the depth analyzed, which indicates that all of the sample has been leached to a similar degree. Additionally, the DTG analysis shows that for leached samples, the peak near 150 °C indicates that the amount of adsorbed water is higher and homogeneous across all three depths when compared to air carbonation and efflorescence exposure. The implications of this observation for the mechanical behavior of the leached samples will be revisited in section 4 below.

3.4. Splitting tensile strength

The splitting test, also known as the Brazilian test, is based on the determination of tensile strength by application of a compressive load in the diametral direction of a cylindrical sample (as is shown in Fig. 6). The results are aligned to the other mechanical test data; the reference exposure condition (RE) showed higher values of splitting tensile strength when compared to the other exposure conditions. The geopolymers with higher contents of soluble silicates (MS_1.5 and MS_1.0) again achieved higher strengths. According to the average values, the splitting tensile strength is approximately 10% of the compressive strength for this sample set. The EF exposure gave similar behavior to air carbonation exposure, except in MS_0.0, where a reduction in strength

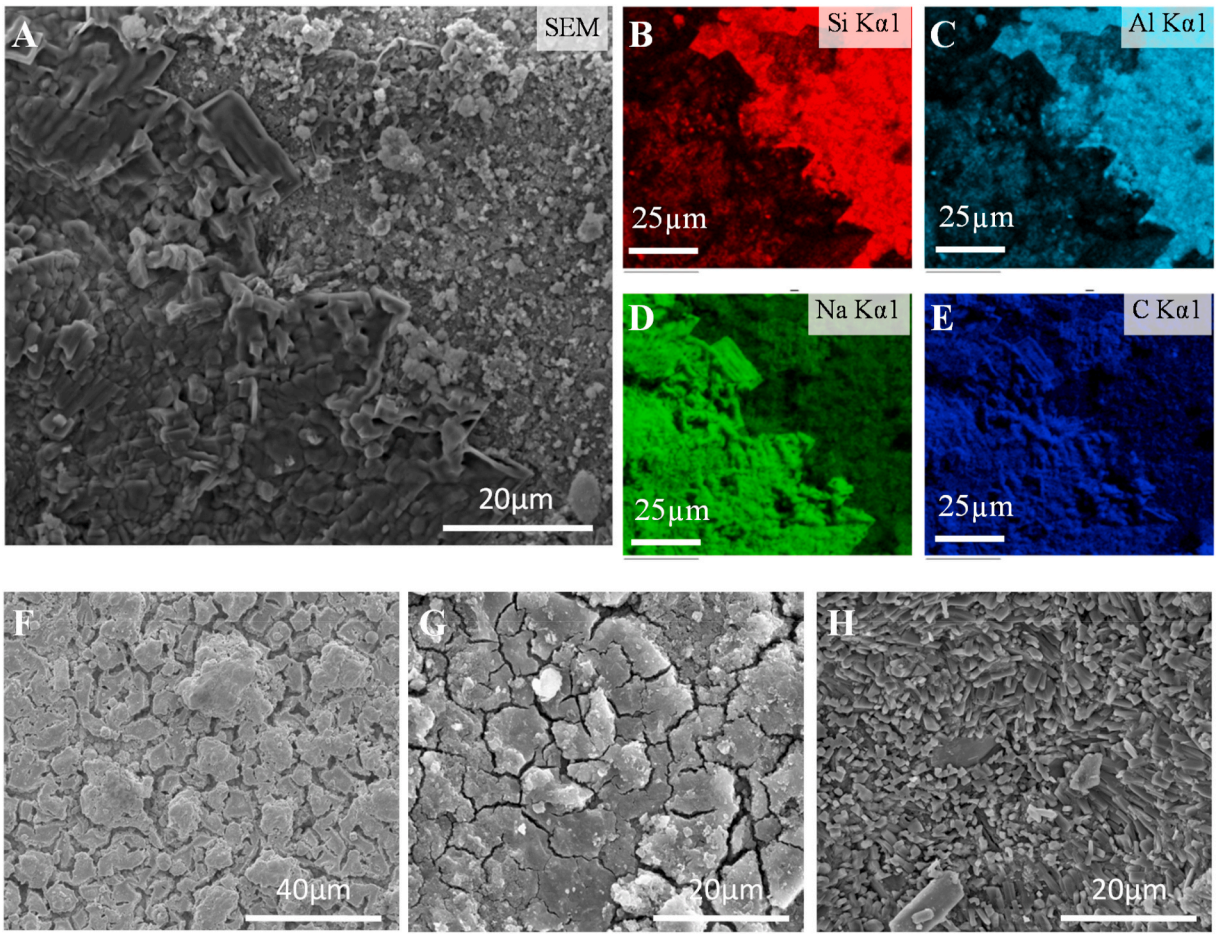

Fig. 10. SEM images and EDS elemental maps of the geopolymer MS_0.5 exposed to air carbonation condition.

of more than 50% was observed. A slight reduction is also identified in the material with thermal curing. The samples exposed to the air carbonation process may show a slight reduction in splitting tensile strength, but this difference cannot be considered statistically significant from the data available. Leaching exposure causes a reduction in splitting tensile strength of around 50% in all systems. Even the geopolymer MS_1.5 is susceptible to the leaching exposure, which is not observed from the compressive strength data. This result is consistent with the trends observed in the flexural strength data, and reflects the susceptibility of geopolymers to loss of tensile properties when exposed to leaching.

3.5. Linear deformation

The results of linear deformation when the samples were exposed to the different exposure conditions are shown in Fig. 7. The dotted line at zero represents a starting point of measurements before each exposure in the samples with 28 days of curing. The lengths of the samples were then measured after exposure to the specific conditions after 28 and 56 days of exposure. In the reference sample the highest shrinkage (~0.25%) is observed in the geopolymers with more silicate in the activator. According to Kuenzel et al. [31], higher Si/Al ratios require more bound water to prevent drying shrinkage, which is consistent with the behavior observed in this study, where the addition of sodium silicate increases the shrinkage.

Under efflorescence conditions, the shrinkage is similar in all ambient-cured samples, with the 50 °C-cured MS_1.0_50° again shrinking less than the others tested. As indicated by Fig. 2 for the MS_1.0 and MS_0.0, efflorescence can induce carbonate formation within the pores and sample degradation; however, as indicated in Fig. 5, the presence of carbonate phases is predominantly superficial. Thus, the internal pressure is not enough to cause an important change in the sample dimension. The samples exposed to natural carbonation show similar shrinkage (between 0.20 and 0.12%), except MS_1.0_50°, which shrinks much less than the corresponding geopolymer MS_1.0 without thermal curing.

Under leaching exposure, a slight expansion is observed in the geopolymers containing more sodium silicate, however this effect cannot be attributed to crystal formation, and it is likely to be related to swelling of the gel as it undergoes microstructural changes during leaches. These changes will be explored in section 4 below.

4. Microstructure and nanostructure

Many of the observations of strength and dimensional changes due to the effect of efflorescence formation, air carbonation and leaching in geopolymers, were identified above as having an important nanostructural and microstructural basis. Therefore, these aspects of the samples were analyzed to elucidate the process of deterioration and identify the origins of this behavior.

4.1. Scanning electron microscopy

The ambient-cured geopolymers (MS_1.5, MS_1.0, MS_0.5 and MS_0.0) were analyzed by SEM after exposure under each of the specified conditions. The images are shown in Fig. 8. The addition of sodium silicate (MS_1.5 and MS_1.0) in the activator induces the formation of a denser microstructure, consistent with the better mechanical

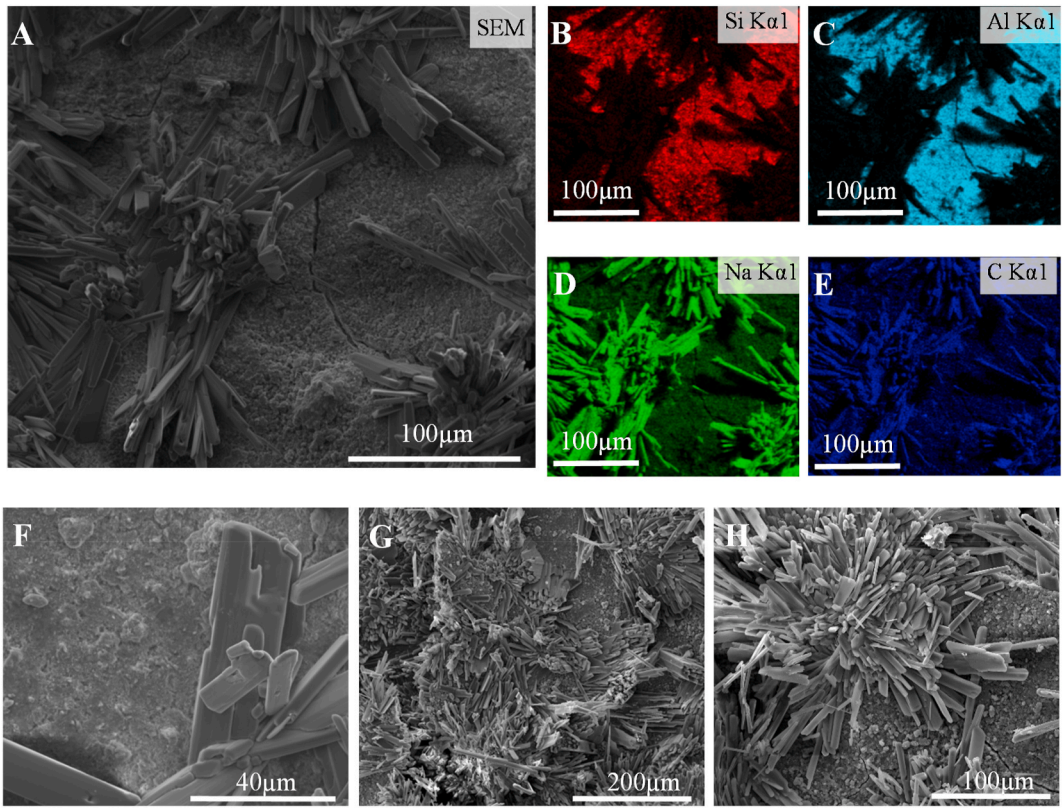

Fig. 11. SEM images and EDS elemental maps of the geopolymer MS_0.5 exposed to efflorescence condition.

performance of these geopolymers than those formulated at lower silicate content, as discussed in section 3. The images obtained correspond to the most external part of the samples exposed to the different conditions (i.e., the darker section shown in Fig. 5A). In the geopolymers with less or no dissolved silicate in the activator (MS_0.5 and MS_0.0), a less consistent matrix is visible, with insufficient dissolution of the precursor, higher porosity and lower density in the geopolymeric matrix.

In general, the MS_1.5 samples do not show marked microstructural differences after exposure under any of the test conditions here. In efflorescence exposure, crystal formation is again observed, along with microstructural deterioration. In the other geopolymer systems, carbonation exposure shows the formation of different sodium carbonate crystals, as also observed in previous studies [19], and superficial shrinkage. In the leaching condition, morphological change within the binder is observed, which indicates that the soluble part of the material is being partially removed, and crystalline reaction products being either altered or deposited.

To evaluate individually the effect of the different exposure conditions, the geopolymers MS_0.5 were investigated in more detail with EDS analysis, Fig. 9 to Fig. 12. According to Fig. 9, for the system MS_0.5 in a reference exposure, the SEM image shows a geopolymer structure containing layered structures that indicate the presence of unreacted metakaolin particles. Using the SEM/EDS mapping technique (B, C, D and E), the homogeneity of the geopolymer matrix is observed in the distribution of Si, Al and Na. Some traces of carbonates are observed, attributed to surface carbonation during sample preparation. As observed in more detail in Fig. 9F–H, the reacted gel has a granular microstructure, however, due to the low silicate content of the activator, this gel does not provide a fully dense matrix. Part of the metakaolin precursor is not reacted, and is therefore retained in the structure as filler.

Under carbonation exposure conditions, is evaluated by SEM image in Fig. 10. In Fig. 10A, the image shows two different morphologies. According to EDS analysis (Fig. 10B–E), the left area (closest part to the exposed surface) is formed mostly of sodium carbonate crystals, with small amounts of Si and Al, while the right area shows the presence of a higher amount of Si and Al and less C, which indicates the presence of carbonated geopolymer gel. Carbonation and exposure to a drying environment (moderate RH) induces cracking as shown in Fig. 10F and G, and the formation of crystals (Fig. 2) due to the excessive alkali movement from the bulk of the sample to the surface induced by the moisture gradient, with a slight contribution caused by sample preparation.

The efflorescence exposure affects the mechanical strength as shown in Figs. 3, Figs. 4 and 6 due to near-surface deterioration and breakage of parts from the samples. As shown in Fig. 11A–E, the crystal is composed of Na and C, in the form of sodium carbonate, growing carbonate crystals on the surface where sodium availability is higher as it migrates along with the water that is evaporating from the sample surface. As observed in Fig. 11F–H, the formation of sodium carbonate, with different shapes and sizes but largely in elongated crystal habits, which are related to the availability of sodium, dissolved carbon dioxide, amount of water and humidity [32,33].

The samples from leaching exposure conditions are shown in Fig. 12, and do not show the formation of carbonate crystals. This is expected due to the high amount of sodium leached when immersed in water, as well as the absence of dissolved CO_2 within the solution. As observed in EDS mapping (Fig. 12B–E), the microstructure is somewhat heterogeneous. As the sample was immersed in water, the presence of carbon is attributed to the contact with air during sample preparation for analysis. In Fig. 12F, a different morphology is observed, and elemental compositions differ between the two marked areas. The left area shows a structure more similar to the reference geopolymer, however, on the right side, the morphology is changed to show non-connected lepispheric type particles, close to spherical and comprising interlocking crystallites [34–36]. In Fig. 12G–H, this structure is again identified. Some studies of zeolite synthesis, particularly those producing chabazite

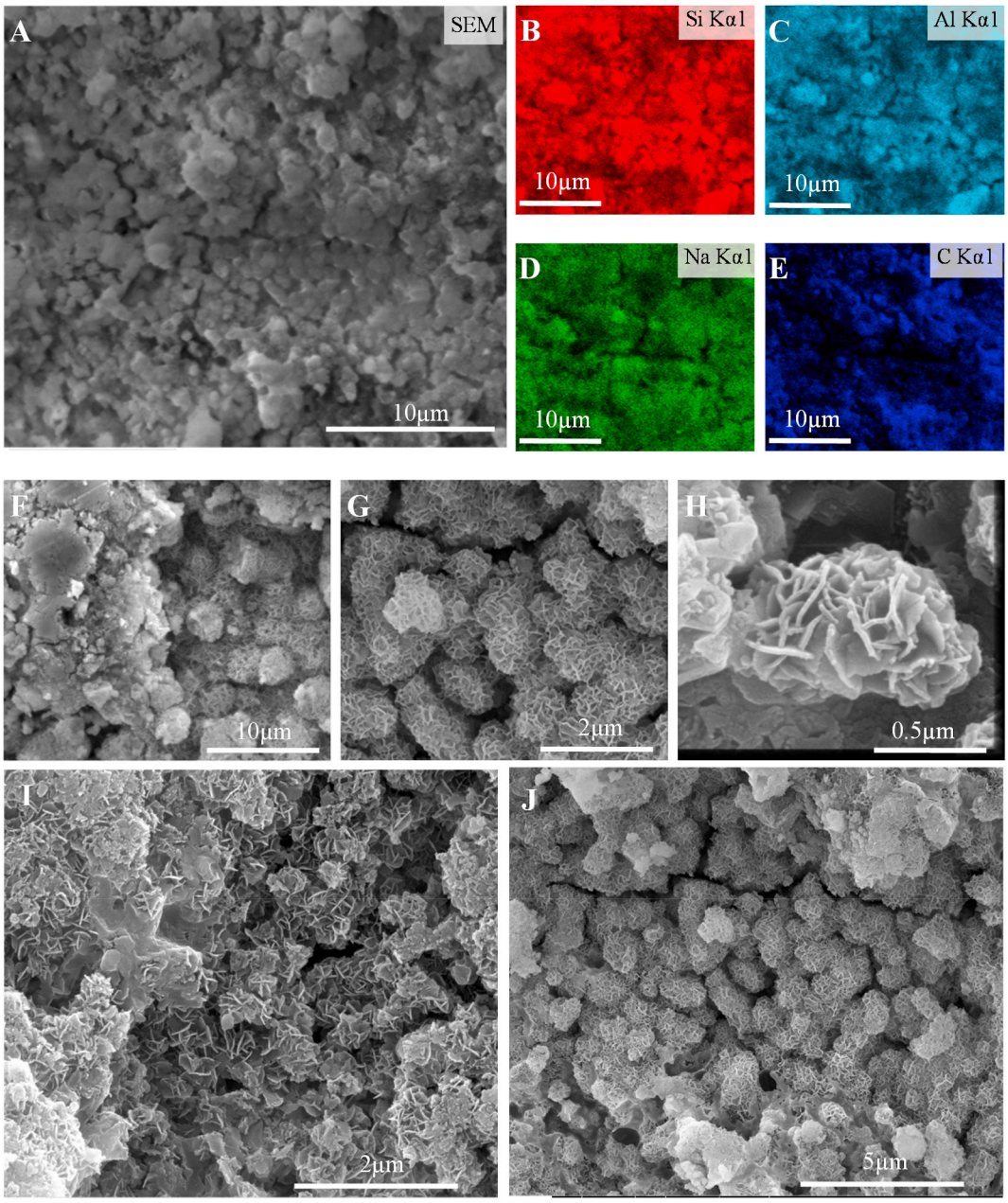

Fig. 12. SEM images and EDS elemental maps of the geopolymer MS_0.5 exposed to leaching conditions.

and sodalite group minerals, show a similar morphology to be characteristic of these minerals [37,38], which indicates that a similar crystallization process and/or product may be observed under the leaching conditions here. The formation of such phases would also be consistent with the observation of high contents of adsorbed (zeolitic) water by DTG in section 3.3 (Fig. 5). Fig. 12I and J shows the remaining part after the leaching exposure, which is constituted of similar morphology to the geopolymer without leaching, and is progressively being transformed in part to lepispheric grains. The morphology formed can also be associated with the mechanical behavior observed, in terms of both flexural and tensile strength. The conversion of some of the gel to the observed granular microstructure reduces the bond between the grains, which directly affects the tensile strength of the material.

Summarizing, the SEM analysis provides evidence of important morphological transformations and helps to identify the phenomena related to each exposure condition. During air carbonation and efflorescence exposure, the formation of crystals or a carbonate layer were observed, and are related to the amount of released compounds. The formation of carbonate crystals within the porous geopolymer structure can generate stress and can affect the mechanical behavior. The leaching exposure condition induced the transformation of morphology within the gel itself.

4.2. Solid state MAS NMR spectroscopy analysis

The **^{27}Al MAS NMR** spectra of the anhydrous metakaolin precursor and the geopolymer sample MS_0.5 in reference, air carbonation, efflorescence and leaching exposure conditions are shown in Fig. 13. The anhydrous metakaolin spectrum exhibits three broad resonances centered at $\delta_{obs} = 6$, 32 and 60 ppm, attributed respectively to aluminum in tetrahedral (IV), pentahedral (V) and octahedral (VI) coordination, which is in agreement with other studies [39,40]. Via the geopolymerization process, Al(V) and Al(VI) are dissolved to react with other elements, and form predominantly Al(IV) species in the

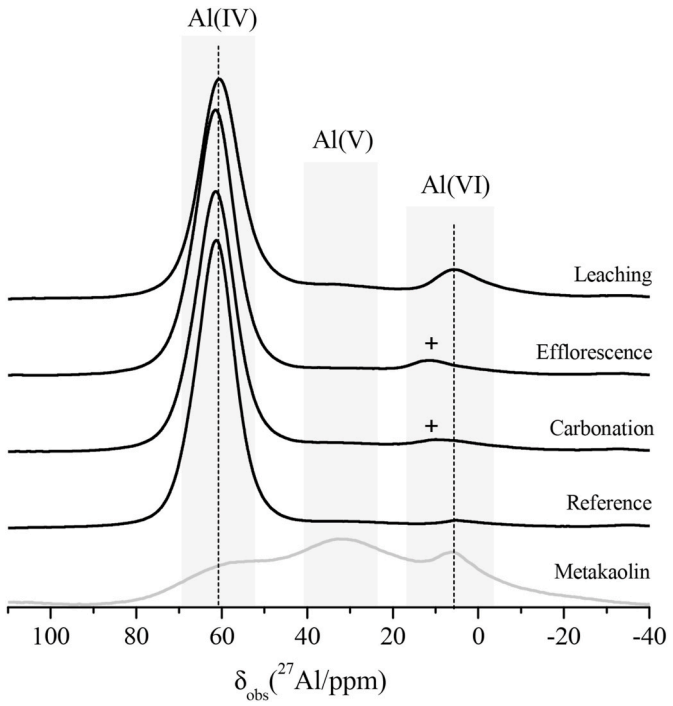

Figs. 13. ^{27}Al MAS NMR spectra of the metakaolin precursor and geopolymer MS_0.5 after reference, air carbonation, efflorescence and leaching exposure conditions.

geopolymer binder [9,39,40]. As reported previously, the presence of aluminum in Al(IV) coordination with a negative charge is charge-balanced mainly by Na^+, which reduces the availability of free alkalis [4,9].

The carbonation of geopolymers in contact with air and the excessive efflorescence formation are attributed to the consumption of free or weakly bounded alkalis to form carbonate phases. This induces the formation of a new broad peak around 10 ppm, in the Al(VI) region (indicated with + in Fig. 13). Under these conditions, Na^+ ions are removed from the charge-balancing sites within the N-A-S-H gel (as a consequence of efflorescence or carbonation), and there is a residual negative charge on the Al ions which must be balanced. As the N-A-S-H gel is now deficient in Na^+, it appears that some of the Al moves into the charge balancing sites in octahedral coordination, becoming the charge balancing extra-framework Al sites observed previously in geopolymer systems [41].

The exposure to different conditions induces some changes to the aluminum sites. The leaching exposure condition reduces the relative intensity of the main peak due to Al(IV) and increases the relative intensities of peaks associated with the remnant unreacted portion of the precursor (Al(V) and Al(VI)). This behavior is consistent with SEM analysis (Fig. 13), which shows a morphology change associated with microstructural transformations.

The **^{29}Si MAS NMR** spectra for the reference geopolymer, and after exposure, are shown in Fig. 14. The different amounts of tetrahedral Si sites present after each exposure type cause changes in the main broad peak, located at −86 ppm for the reference system, −84.9 ppm for air carbonation, −84.9 ppm for efflorescence conditions, and −85.6 ppm for leaching exposure. This broad peak is composed of Q^4(mAl) species, which are deconvoluted using Gaussian distributions to simulate resonances at δ_{iso} = −85 (Q^4(4Al)), −90 (Q^4(3Al)), −95 (Q^4(2Al)), −100 (Q^4(1Al)), −105 (Q^4(0Al)) ppm. The resonance with highest intensity in all spectra is that due to Q^4(4Al) sites, consistent with the nominal Al/Si ratio and the ^{27}Al MAS NMR data, where the presence of aluminum is predominantly in tetrahedral form.

The **^{23}Na MAS NMR** spectra of the reference and exposed geopolymers are shown in Fig. 15. The geopolymers exhibit a single broad resonance between −2.48 and −4.5 ppm, which can be attributed to sodium associated to the aluminum-centered tetrahedra in a charge balancing role, providing the Na^+ necessary for the equilibrium of the gel framework [39,42]. According to Duxson et al. [39], the resonances around −4 ppm are attributed to sodium associated to the aluminum in charge-balancing roles, while resonances near to 0 ppm can be attributed to mobile sodium atoms located in the pore solution. In some cases, this would appear as a sharp near to 0 ppm (as ions in the pore solution are highly mobile). In this study, this resonance is not observed, indicating that all Na is bound in a charge balancing site. Interestingly, there are no obvious resonances due to sodium carbonate phases (which would appear around 5 ppm and around −15 to −20 ppm) [43], however, for the efflorescence and carbonated samples there appears to be a broad shoulder at about 2 ppm, which could be due to sodium carbonate overlapping with the main resonance due to sodium in charge balancing site. The absence of an intense peak associated with carbonate may be related to the preparation of the sample, where the previously formed carbonate may dissolve. After leaching exposure condition the main broad peak is observed in −4.5 ppm, indicating Na^+ is mostly associated to the tetrahedral aluminum Al(IV).

4.3. XRD

Fig. 16 shows the XRD data for metakaolin, and for geopolymers exposed to different conditions. In the metakaolin precursor, the main signal is observed as a broad feature between 10 and 30° 2θ, attributed to the amorphous part of the material. Some traces of anatase (TiO_2, Powder Diffraction File, PDF, # 00-021-1272) and halloysite ($Al_2Si_2O_5(OH)_4$, PDF# 00-029-1489) are observed, indicating a crystalline and nonreactive part in the raw material. After the geopolymerisation process, the amorphous feature is reduced and shifted to higher values, indicating the consumption of metakaolinite and formation of N-A-S-H type gel. The crystalline phases (anatase and halloysite) remain in the structure.

After exposure, the main difference is observable after efflorescence conditions (EF), where the formation of crystals is observed: sodium carbonate (Na_2CO_3, PDF # 01-086-0301), thermonatrite ($Na_2CO_3{\cdot}H_2O$, PDF # 01-070-2148) and natron ($Na_2CO_3{\cdot}10H_2O$, PDF # 00-015-0800). This formation is more visible in MS_0.5-EF and MS_0.0-EF, which were the systems with the highest formation of external efflorescence. The same products were also observed in other studies [14,15,44].

In air carbonation exposure, even with the visible superficial carbonation observed in Fig. 5, it is not possible to identify a massive formation of carbonate phases, probably due to the low amount of carbonates compared to the total mass of the sample. After leaching exposure, the microstructural transformation is visible by SEM, however, the formation of new crystalline phases is not identifiable by XRD. The leaching exposure does not generate a new crystalline phase, the SEM presented in Fig. 12 indicates the dissolution of the part of the gel, resulting in different morphology.

4.4. MIP

The MIP analysis is shown in Fig. 17. Even with its known limitations related to the ink bottle effect [45] and the presence of different sizes and shapes of pores, which will increase the measured volume of very small pores at the expense of some larger pores [46], this technique is widely used to identify differences in pore sizes when different conditions or parameters are assessed for comparison purposes. By MIP it is possible to estimate the total accessible porosity (Fig. 17A), where the lower values are observed in high sodium silicate geopolymers. This property is consistent with mechanical behavior shown in Figs. 3, Figs. 4 and 6, indicating the relationships between mechanical strength and porosity. This behavior is associated to the formation of less and smaller pores [47,48]. There is a reduction of porosity due to air carbonation,

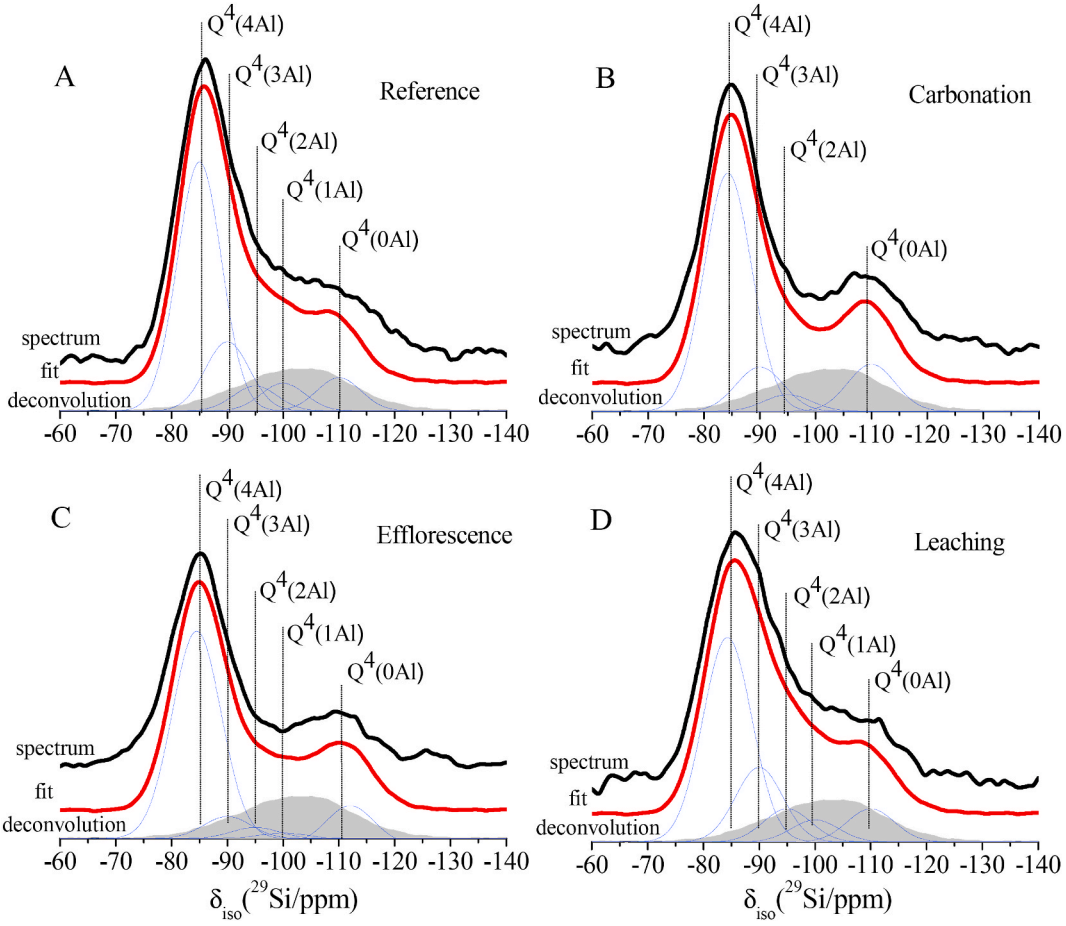

Figs. 14. ^{29}Si MAS NMR of spectrum (black lines), simulation (red lines) and spectral deconvolution (blue lines for reaction products; grey shaded area for remnant precursor) for geopolymer MS_0.5 under reference, air carbonation, efflorescence, and leaching exposure conditions. (For interpretation of the references to colour in this figure legend, the reader is referred to the Web version of this article.)

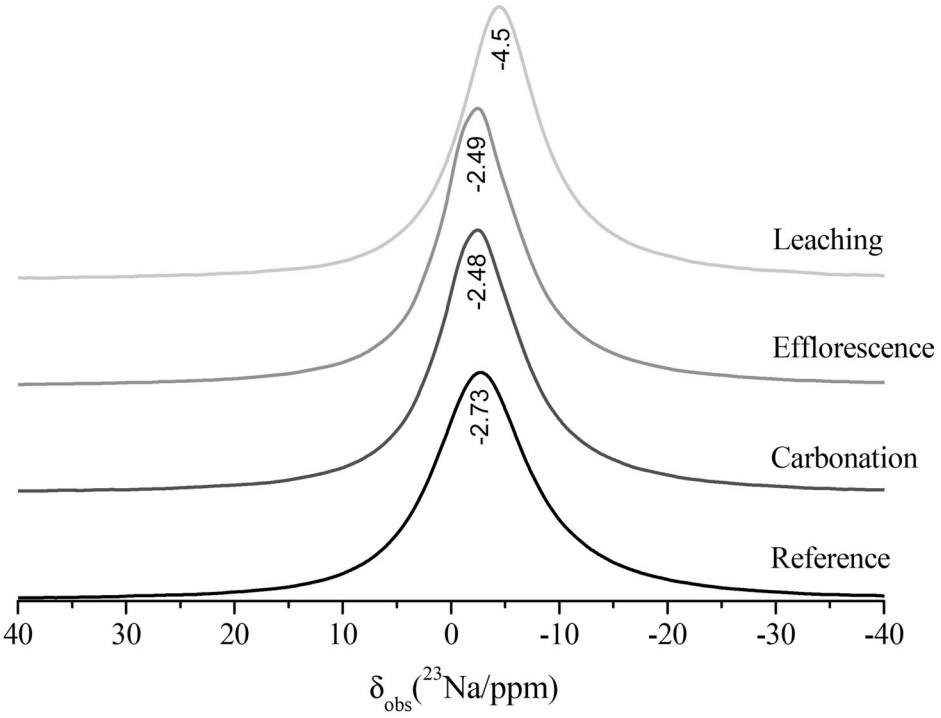

Figs. 15. ^{23}Na MAS NMR spectra of the geopolymer binder MS_0.5 in reference conditions and after exposure.

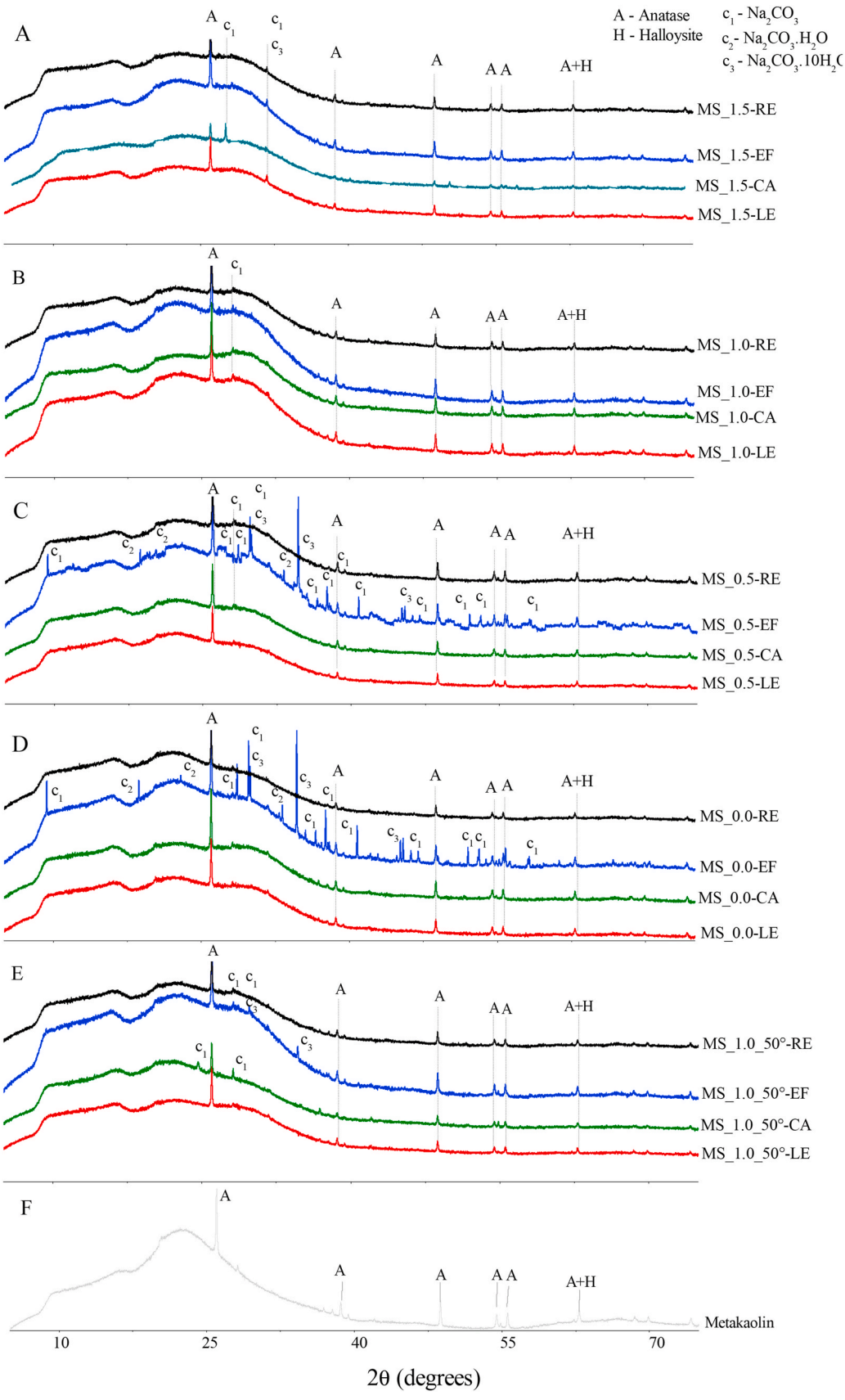

Fig. 16. XRD patterns of the metakaolin geopolymers after exposure; A: MS_1.5, B: MS_1.0, C: MS_0.5, D: MS_0.0, E: MS_1.0_50°, F: Metakaolin. Synchrotron X-ray diffraction data (12 keV) have been converted to equivalent Cu Kα 2θ angles for plotting. Step-like features in the MS_0.5-EF diffractogram are attributed to minor instabilities in the beamline during data collection, but do not interfere with the qualitative phase identification conducted.

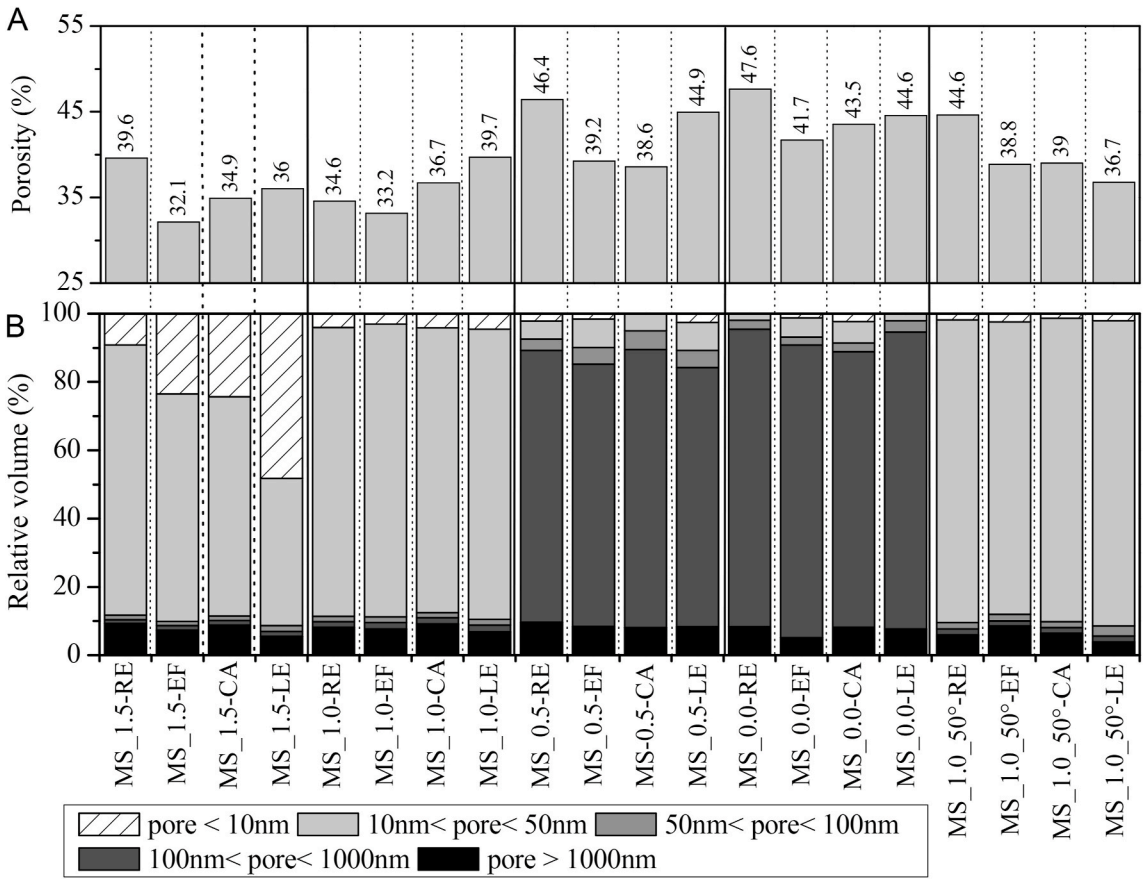

Fig. 17. Porosity and pore size distribution of geopolymers, measured by MIP. A. Porosity (%), B. relative volume of pore size distribution (%).

efflorescence formation and leaching, except for the geopolymer MS_1.0, where the porosity increased due to air carbonation and leaching. The porosity reduction is more sensitive to air carbonation and efflorescence than leaching, which aids in identifying that it can be associated with the formation of carbonate crystals, especially in the systems MS_0.5 and MS_0.0, consistent with the carbonate formation identified by XRD (Fig. 16).

Using the relative volume of pores in different size ranges (Fig. 17B), it is possible to observe the effect of design parameters and exposure conditions on pore size formation. A high content of sodium silicate leads to the formation of small pore sizes when compared to the geopolymers with low MS, this increasing can reduce de pore size, and consequently, decrease the ions leaching [49]. The MS_1.5 contains mainly pores smaller than 50 nm, with a large volume of pores smaller than 10 nm. Similar behavior is observed in the geopolymer MS_1.0, but with a lower content of pores below 10 nm, both with and without thermal curing. On the other hand, the geopolymers MS_0.5 and MS_0.0 present pores mainly in the range between 100 nm and 1000 nm, similar to other studies [50,51]. This behavior is also consistent to mechanical properties measured. Under the different exposure conditions, the geopolymers MS_1.5 showed the more notable changes, with the presence of smaller pores in air carbonation, efflorescence and leaching when compared to the reference exposure.

The presence of small pores also indicates more gel formation, inducing a denser and stronger structure. The presence of pores with smaller diameters is important for durability, considering that the diffusion of aggressive agents inside the binder structure is usually more rapid through larger pores [52].

4.5. X-ray microtomography

Fig. 18 shows the 3D tomographic image renderings for the geopolymer assessed (MS_0.0) under reference, efflorescence and leaching exposure conditions; this was selected as it was the system with higher degradation after the exposure conditions. The air entrained during mixing is identified easily as large and spherical bubbles, bigger than 10 μm (Fig. 18), which were extracted selectively using a watershed filter segmentation technique [26]. The volume fraction of these voids is calculated to be between 2.6 ± 0.3% for the geopolymers assessed. This value will not be considered in the total porosity discussion below, due to the size and origin of these voids. The large pores (with sizes higher than 4 μm) were assessed by the selection of point-based threshold based on a high grey level transition ("or transition point") [53]. The calculated volume fraction of pores between 4 μm and 10 μm is 3.3, 1.4 and 1.2%, respectively. Transition point identification based on the grey-scale histogram is a method used often for segmentation. However, this technique may not be appropriate for the geopolymer materials studied here, since their porosity networks exhibit pore sizes smaller than the voxel resolution (Fig. 17), and the sample produces a wide range of greyscale intensities for different phases (unreacted and partially unreacted particles, as well as reacted products) [54,55]. Taking into account that the images acquired in the XRμT are also limited in resolution (0.84 μm per voxel/pixel), a detailed analysis of pore network geometry is not reliable for this material when studied at this resolution. The images and pore volume reported here correspond to voids with sizes larger than 4 μm, where the statistics and consistency during the application of the segmentation algorithm showed coherence between images, results derived from other techniques, and previous reports [54,55]. On the other hand, the voids (or air bobbles identified) are generated during mixing and sample production, and can be

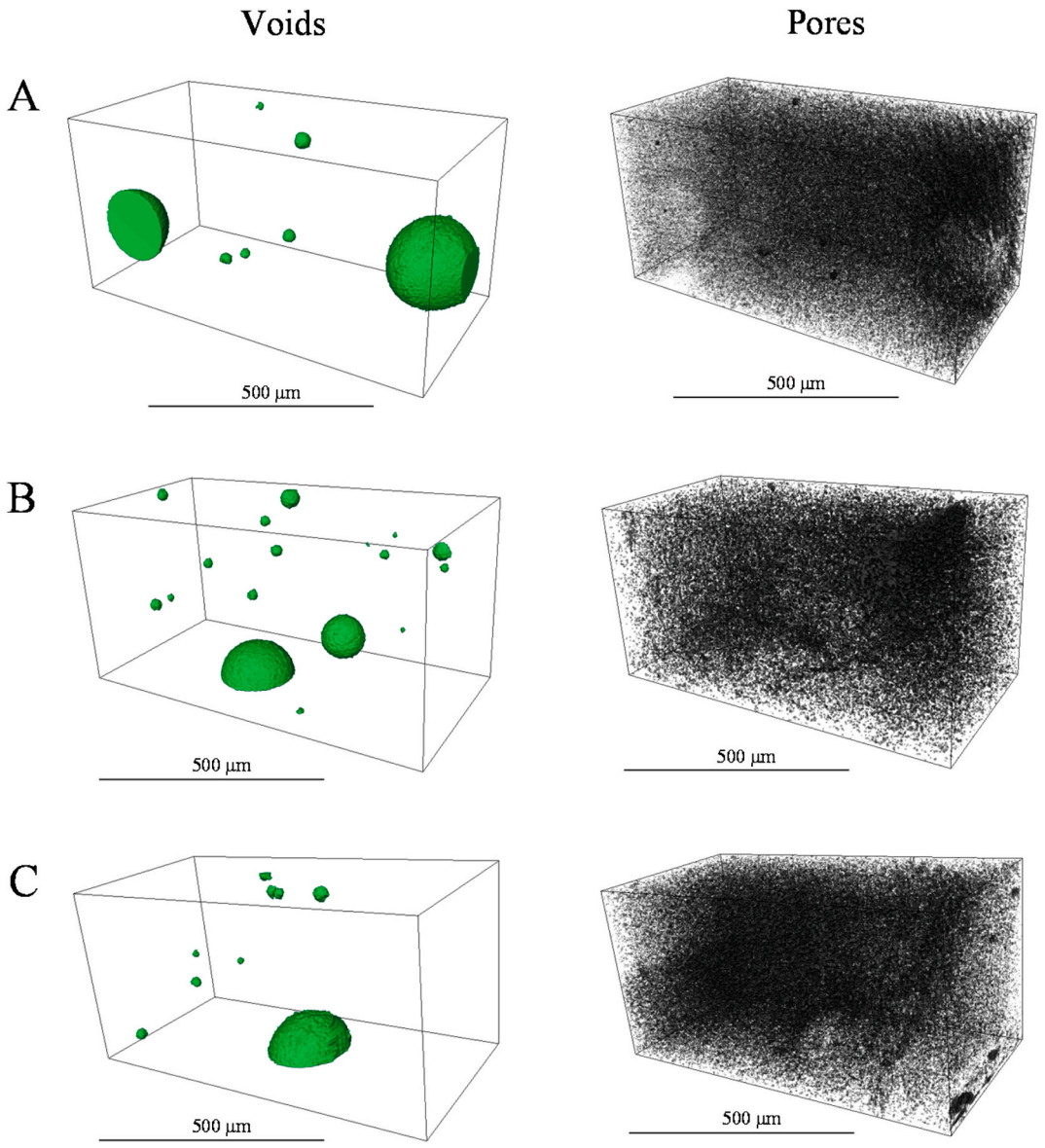

Fig. 18. Images of voids and pores of a prismatic region of the geopolymer MS_0.0 exposed to: A. Reference, B. Efflorescence, C. Leaching.

attributed to the insufficiency of air removal by vibration here, as a result of the high viscosity of the fresh geopolymer paste [56].

This analysis aims to identify if the porosity or the gel structure changes due to the exposure of the geopolymers to the process of efflorescence and leaching. The complete distinction between the phases (unreacted and partially reacted particles, N-A-S-H gel and microporosity) is quite difficult and represents the main limitation of XRμT for this type of material.

5. Conclusions

This study evaluated separately the effects of air carbonation, efflorescence formation, and leaching in metakaolin based geopolymers on mechanicals strength and micro/nanostructure.

The condition of exposure to air carbonation induces the process of carbonation associated with the efflorescence formation. This phenomenon occurs in the first layers of the material and affects the mechanical performance of geopolymers. The main property affected is compressive strength. Geopolymers containing more sodium silicate are less susceptible to changes in mechanical strength. According to the influence of porosity, the larger pores allows the migration of moisture containing dissolved alkalis to the free surfaces of the sample, and thus induces the carbonate crystals to grow.

Efflorescence formation in geopolymers is strongly dependent on design parameters, where the addition of sodium silicate associated with the correct content of alkali can reduce the extent of efflorescence formation. It is also a process that can affect all mechanical properties, especially compressive strength, which is strongly affected in some geopolymers. This effect is associated with excessive superficial deterioration and crystal formation within the pores, also associated to internal (near-surface) carbonation, which may generate internal stress greater than the tensile strength of the material and causes the rupture of fragments or parts. The main products of efflorescence are sodium carbonates in hydrous or anhydrous forms, which grow on the surface in different shapes and sizes.

Leaching can be indicated as the first process associated with efflorescence formation. This exposure condition induces the removal of free or weakly bonded alkalis, which may affect the mechanical and microstructural properties. The flexural and tensile strength of geopolymers are sensitive to exposure to leaching conditions. The excessive removal of exchangeable sodium can change the equilibrium of aluminum in the framework structure, and consequently, the stability of some phases in

the gel. The local densifications of the gel resulted in the formation of a structure based on non-connected grains. A morphological transformation of gel can be observed by SEM. The addition of sodium silicate provides an improvement in the mechanical properties, and the microstructure evolves when immersed in water.

Declaration of competing interest

The authors declare that they have no known competing financial interests or personal relationships that could have appeared to influence the work reported in this paper.

Acknowledgements

M.A. Longhi is grateful for the financial support of CAPES and of SWE 203750/2017–9. The participation of A. P. Kirchheim Brazilian authors was sponsored by CNPq (Brazilian National Council for Scientific and Technological Development) through the research fellowships PQ2017 305530/2017–8. The participation of E. D. Rodríguez was supported by CNPq research fellowship PQ 309885/2020–5. The participation of B. Walkley was supported by the Engineering and Physical Sciences Research Council (UK) through grant EP/P013171/1. The participation of Z. Zhang was supported by National Scientific Foundation of China (51878263, U2001225). The authors would like to thank the LNNano for technical support during electron microscopy work (proposal SEM 24390), as well as the LNLS for the use of the IMX and XRD1 beamline (proposals 20180210, 20180361), and Dr Sandra van Meurs, Department of Chemistry, The University of Sheffield, for assistance in acquiring the NMR data and insightful discussions related to this work.

References

[1] P. Duxson, J.L. Provis, G.C. Lukey, J.S.J. van Deventer, The role of inorganic polymer technology in the development of 'green concrete, Cement Concr. Res. 37 (2007) 1590–1597, https://doi.org/10.1016/j.cemconres.2007.08.018.
[2] J.L. Provis, Geopolymers and other alkali activated materials: why, how, and what? Mater. Struct. 47 (2013) 11–25, https://doi.org/10.1617/s11527-013-0211-5.
[3] P. Duxson, J.L. Provis, G.C. Lukey, S.W. Mallicoat, W.M. Kriven, J.S.J. van Deventer, Understanding the relationship between geopolymer composition, microstructure and mechanical properties, Colloids Surfaces A Physicochem. Eng. Asp. 269 (2005) 47–58, https://doi.org/10.1016/j.colsurfa.2005.06.060.
[4] A. Fernández-Jiménez, A. Palomo, I. Sobrados, J. Sanz, The role played by the reactive alumina content in the alkaline activation of fly ashes, Microporous Mesoporous Mater. 91 (2006) 111–119, https://doi.org/10.1016/j.micromeso.2005.11.015.
[5] M.R. Rowles, Brian H. O'Connor, Chemical and structural microanalysis of aluminosilicate geopolymers synthesized by sodium silicate activation of metakaolinite ReadCube articles, J. Am. Ceram. Soc. 92 (2009) 2354–2361.
[6] B.H. O'connor, M.R. Rowles, J.V. Hanna, K.J. Pike, M.E. smith, Al Si, 1 H and 23 Na MAS NMR study of the bonding character in aluminosilicate inorganic polymers 27, Appl. Magentic Reson. 32 (2007) 663–689, https://doi.org/10.1007/s00723-007-0043-y.
[7] E. Najafi, A. Allahverdi, J.L. Provis, Efflorescence control in geopolymer binders based on natural pozzolan, Cement Concr. Compos. 34 (2012) 25–33, https://doi.org/10.1016/j.cemconcomp.2011.07.007.
[8] Z. Zhang, J.L. Provis, A. Reid, H. Wang, Fly ash-based geopolymers: the relationship between composition, pore structure and efflorescence, Cement Concr. Res. 64 (2014) 30–41.
[9] M.A. Longhi, B. Walkley, E.D. Rodríguez, A.P. Kirchheim, Z. Zhang, H. Wang, New selective dissolution process to quantify reaction extent and product stability in metakaolin-based geopolymers, Compos. B Eng. 176 (2019) 107172, https://doi.org/10.1016/j.compositesb.2019.107172.
[10] Y.F. Houst, F.H. Wittmann, Influence of porosity and water content on the diffusivity of CO2 and O2 through hydrated cement paste, Cement Concr. Compos. 24 (1994) 1165–1176.
[11] K. Arbi, M. Nedeljkovic, Y. Zuo, G. Ye, A review on the durability of alkali-activated fly ash/slag Systems : advances, issues, and perspectives, Ind. Eng. Chem. Res. 55 (2016) 5439–5453, https://doi.org/10.1021/acs.iecr.6b00559.
[12] S.A. Bernal, J.L. Provis, Durability of alkali-activated materials: progress and perspectives, J. Am. Ceram. Soc. 97 (2014) 997–1008, https://doi.org/10.1111/jace.12831.
[13] Z. Zhang, J.L. Provis, X. Ma, A. Reid, H. Wang, Efflorescence and subflorescence induced microstructural and mechanical evolution in fly ash-based geopolymers, Cement Concr. Compos. 92 (2018) 165–177, https://doi.org/10.1016/j.cemconcomp.2018.06.010.
[14] F. Škvára, L. Kopecký, L. Myšková, V.Í.T. Šmilauer, L. Alberovská, L. Vinšová, Aluminosilicate polymers - influence of elevated temperatures, efflorescence, Ceram. - Silikaty. 53 (2009) 276–282.
[15] O. Burciaga-Díaz, J.I. Escalante-García, R. Arellano-Aguilar, A. Gorokhovsky, Statistical analysis of strength development as a function of various parameters on activated metakaolin/slag cements, J. Am. Ceram. Soc. 93 (2010) 541–547, https://doi.org/10.1111/j.1551-2916.2009.03414.x.
[16] A. Arnold, K. Zehnder, "Salt weathering on monuments,", in: I' Simposio Internazionale Bari., 1989.
[17] A. Arnold, K. Zehnder, Monitoring wall paintings affected by soluble salts, Conserv. Wall Paint, in: Proc. A Symp. Organ. by Court. Inst. Art Getty Conserv. Institute, London, July 13–16, 1987, 1991, pp. 103–135. http://192.215.101.9/conservation/publications_resources/pdf_publications/wall_paintings.pdf#page=130.
[18] X. Yao, T. Yang, Z. Zhang, Compressive strength development and shrinkage of alkali-activated fly ash–slag blends associated with efflorescence, Mater. Struct. Constr. 49 (2016) 2907–2918, https://doi.org/10.1617/s11527-015-0694-3.
[19] M.A. Longhi, E.D. Rodríguez, B. Walkley, Z. Zhang, A.P. Kirchheim, Metakaolin-based geopolymers: relation between formulation, physicochemical properties and efflorescence formation, Compos. B Eng. 182 (2020), https://doi.org/10.1016/j.compositesb.2019.107671.
[20] D. Massiot, F. Fayon, M. Capron, I. King, S. Le Calvé, B. Alonso, J.-O.O. Durand, B. Bujoli, Z. Gan, G. Hoatson, Modelling one- and two-dimensional solid-state NMR spectra, Magn. Reson. Chem. 40 (2002) 70–76, https://doi.org/10.1002/mrc.984.
[21] P. Duxson, J.L. Provis, G.C. Lukey, F. Separovic, J.S.J. Van Deventer, Si NMR Study of Structural Ordering in Aluminosilicate Geopolymer Gels, 2005, pp. 3028–3036, https://doi.org/10.1021/la047336x.
[22] A.M.G. Carvalho, D.H.C. Araújo, H.F. Canova, C.B. Rodella, D.H. Barrett, S. L. Cuffini, R.N. Costa, R.S. Nunes, X-ray powder diffraction at the XRD1 beamline at LNLS, J. Synchrotron Radiat. 23 (2016) 1501–1506, https://doi.org/10.1107/s1600577516012686.
[23] A.M.G. Carvalho, R.S. Nunes, A.A. Coelho, X-ray powder diffraction of high-Absorption materials at the XRD1 beamline off the best conditions: application to (Gd, Nd)5Si4 compounds, Powder Diffr. 32 (2017) 10–14, https://doi.org/10.1017/S0885715616000646.
[24] F.C. Lussani, R.F.D.C. Vescovi, T.D. De Souza, C.A.P. Leite, C. Giles, A versatile x-ray microtomography station for biomedical imaging and materials research, Rev. Sci. Instrum. 86 (2015), https://doi.org/10.1063/1.4922607.
[25] R.A. Brooks, G. Di Chiro, Beam hardening in X-ray reconstructive tomography, Phys. Med. Biol. 21 (1976) 390–398, https://doi.org/10.1088/0031-9155/21/3/004.
[26] C. de Lima, E. Salomão Helou, Fast projection/backprojection and incremental methods applied to synchrotron light tomographic reconstruction, J. Synchrotron Radiat. 25 (2018) 248–256, https://doi.org/10.1107/S1600577517015715.
[27] R.R. Lloyd, J.L. Provis, J.S.J. Van Deventer, Pore solution composition and alkali diffusion in inorganic polymer cement, Cement Concr. Res. 40 (2010) 1386–1392, https://doi.org/10.1016/j.cemconres.2010.04.008.
[28] P. Duxson, a. Fernández-Jiménez, J.L. Provis, G.C. Lukey, a. Palomo, J.S. J. Deventer, Geopolymer technology: the current state of the art, J. Mater. Sci. 42 (2006) 2917–2933, https://doi.org/10.1007/s10853-006-0637-z.
[29] Z. Zhang, H. Wang, J.L. Provis, F. Bullen, A. Reid, Y. Zhu, Quantitative kinetic and structural analysis of geopolymers. Part 1. The activation of metakaolin with sodium hydroxide, Thermochim. Acta 539 (2012) 23–33, https://doi.org/10.1016/j.tca.2012.03.021.
[30] F. Škvára, V. Šmilauer, P. Hlaváček, L. Kopecký, Z. Cílová, A weak alkali bond in (N, K)-A-S-H gels: evidence from leaching and modeling, Ceram. - Silikaty. 56 (2012) 374–382.
[31] C. Kuenzel, L.J. Vandeperre, S. Donatello, A.R. Boccaccini, C. Cheeseman, Ambient temperature drying shrinkage and cracking in metakaolin-based geopolymers, J. Am. Ceram. Soc. 95 (2012) 3270–3277, https://doi.org/10.1111/j.1551-2916.2012.05380.x.
[32] W.H. Taft, Chapter 3 Physical chemistry of formation of sodium carbonates, in: Developments in Sedimentology, vol. 9, Elsevier, 1967, pp. 151–167. Part B.
[33] L.D. Whittig, P. Janitzky, Mechanisms of formations of sodium carbonate in soils, J. Soil Sci. 14 (1963) 322–333, https://doi.org/10.1111/j.1365-2389.1963.tb00956.x.
[34] Y. Deng, M. Flury, J.B. Harsh, A.R. Felmy, O. Qafoku, Cancrinite and sodalite formation in the presence of cesium, potassium, magnesium, calcium and strontium in Hanford tank waste simulants, Appl. Geochem. 21 (2006) 2049–2063, https://doi.org/10.1016/j.apgeochem.2006.06.019.
[35] Y. Deng, J.B. Harsh, M. Flury, J.S. Young, J.S. Boyle, Mineral formation during simulated leaks of Hanford waste tanks, Appl. Geochem. 21 (2006) 1392–1409, https://doi.org/10.1016/j.apgeochem.2006.05.002.
[36] S. Choi, G. Crosson, K.T. Mueller, S. Seraphin, J. Chorover, Clay mineral weathering and contaminant dynamics in a caustic aqueous system II. Mineral transformation and microscale partitioning, Geochem. Cosmochim. Acta 69 (2005) 4437–4451, https://doi.org/10.1016/j.gca.2005.04.004.
[37] Z. Huo, X. Xu, Z. Lv, Thermal Study of NaP Zeolite with Different Morphologies, 2013, pp. 365–369, https://doi.org/10.1007/s10973-012-2301-y.
[38] J. Luo, H. Zhang, J. Yang, Hydrothermal synthesis of sodalite on alkali-activated coal fly ash for removal of lead ions, Procedia Environ. Sci. 31 (2016) 605–614, https://doi.org/10.1016/j.proenv.2016.02.105.
[39] P. Duxson, G.C. Lukey, F. Separovic, J.S.J. van Deventer, Effect of alkali cations on aluminum incorporation in geopolymeric gels, Ind. Eng. Chem. Res. 44 (2005) 832–839, https://doi.org/10.1021/ie0494216.

[40] B. Walkley, J.L. Provis, Solid-state nuclear magnetic resonance spectroscopy of cements, Mater. Today Adv. 1 (2019) 100007, https://doi.org/10.1016/j.mtadv.2019.100007.
[41] B. Walkley, G.J. Rees, R.S. Nicolas, J.S.J. Van Deventer, J. V Hanna, J.L. Provis, New structural model of hydrous sodium aluminosilicate gels and the role of charge-balancing extra-framework Al, J. Phys. Chem. C 4 (2018) 5673–5685, https://doi.org/10.1021/acs.jpcc.8b00259.
[42] B. Walkley, R. San Nicolas, M.-A. Sani, J.D. Gehman, J.S.J. van Deventer, J. L. Provis, Phase evolution of Na_2O–Al_2O_3 –SiO_2 –H_2O gels in synthetic aluminosilicate binders, Dalton Trans. 45 (2016) 5521–5535, https://doi.org/10.1039/C5DT04878H.
[43] A.R. Jones, R. Winter, G. Neville Greaves, I.H. Smith, ^{23}Na, ^{29}Si, and ^{13}C MAS NMR investigation of glass-forming reactions between Na2CO3 and SiO 2, J. Phys. Chem. B 109 (2005) 23154–23161, https://doi.org/10.1021/jp053953y.
[44] Z. Zhang, J.L. Provis, A. Reid, H. Wang, Fly ash-based geopolymers: the relationship between composition, pore structure and efflorescence, Cement Concr. Res. 64 (2014) 30–41, https://doi.org/10.1016/j.cemconres.2014.06.004.
[45] K. Scrivener, R. Snellings, B. Lothenbach, A Practical Guide to Microstructural Analysis of Cementitious Materials - Chapter 5: Thermogravimetrix Analysis, Taylon and, CRC press, Boca Raton, 2016.
[46] S. Diamond, Mercury porosimetry an inappropriate method for the measurement of pore size distributions in, cement-based materials 30 (2000) 1517–1525.
[47] K. Okada, A. Ooyama, T. Isobe, Y. Kameshima, A. Nakajima, K.J.D. MacKenzie, Water retention properties of porous geopolymers for use in cooling applications, J. Eur. Ceram. Soc. 29 (2009) 1917–1923, https://doi.org/10.1016/j.jeurceramsoc.2008.11.006.
[48] Z. Zhang, X. Yao, H. Zhu, Potential application of geopolymers as protection coatings for marine concrete II. microstructure and anticorrosion mechanism, Appl. Clay Sci. 49 (2010) 7–12, https://doi.org/10.1016/j.clay.2010.04.024.
[49] K. Sun, X. Peng, S. Wang, L. Zeng, P. Ran, G. Ji, Effect of nano-SiO_2 on the efflorescence of an alkali-activated metakaolin mortar, Construct. Build. Mater. 253 (2020) 118952, https://doi.org/10.1016/j.conbuildmat.2020.118952.
[50] K. Gao, K.-L. Lin, D. Wang, H.-S. Shiu, C.-L. Hwang, T.-W. Cheng, Effects of nano-SiO_2 on setting time and compressive strength of alkaliactivated metakaolin-based geopolymer, Open Civ. Eng. J. 7 (2013) 84–92, https://doi.org/10.2174/1874149501307010084.
[51] S.M. Rao, I.P. Acharya, Mercury intrusion porosimetry studies with geopolymers, Indian Geotech. J. 47 (2017) 495–502, https://doi.org/10.1007/s40098-017-0245-7.
[52] E.D. Rodríguez, S.A. Bernal, J.L. Provis, J. Paya, J.M. Monzo, M. Victoria, Cement & Concrete Composites Effect of nanosilica-based activators on the performance of an alkali-activated fly ash binder 35 (2013) 1–11.
[53] J.L. Provis, R.J. Myers, C.E. White, V. Rose, J.S.J. Van Deventer, X-ray microtomography shows pore structure and tortuosity in alkali-activated binders, Cem, Concr. Res. 42 (2012) 855–864, https://doi.org/10.1016/j.cemconres.2012.03.004.
[54] J.L. Provis, R.J. Myers, C.E. White, V. Rose, J.S.J. Van Deventer, J.S.J. van Deventer, Cement and Concrete Research X-ray microtomography shows pore structure and tortuosity in alkali-activated binders, Cement Concr. Res. 42 (2012) 855–864, https://doi.org/10.1016/j.cemconres.2012.03.004.
[55] S. Das, P. Yang, S.S. Singh, J.C.E. Mertens, X. Xiao, N. Chawla, N. Neithalath, Effective properties of a fly ash geopolymer: synergistic application of X-ray synchrotron tomography, nanoindentation, and homogenization models, Cement Concr. Res. 78 (2015) 252–262, https://doi.org/10.1016/j.cemconres.2015.08.004.
[56] D.W. Zhang, D. min Wang, Z. Liu, F. zhu Xie, Rheology, agglomerate structure, and particle shape of fresh geopolymer pastes with different NaOH activators content, Construct. Build. Mater. 187 (2018) 674–680, https://doi.org/10.1016/j.conbuildmat.2018.07.205.